Multi-scale modelling of fire in accelerator tunnels: a CERN case study

Melchior Schepers

Fire Safety Engineering
Lund University
Sweden

Report 5575, Lund 2018

Master Thesis in Fire Safety Engineering

Multi-scale modelling of fire in accelerator tunnels: a CERN case study

Melchior Schepers

Report 5575
ISRN: LUTVDG/TVBB—5575--SE

Number of pages: 96
Illustrations: 63

Keywords
Multi-scale modelling, CFD, tunnel fires, FDS, CERN, particle accelerator

Abstract

Multi-scale modelling is a novel approach to fire modelling in situations where the size of the domain prevents it from being modelled completely in 3D. By splitting the domain in a 1D and 3D portion multi-scale modelling allows for much faster simulations which still adhere to the correct boundary conditions. In this thesis the multi-scale methodology is applied to the LHC accelerator in use at CERN using the HVAC capabilities of FDS. The theoretical foundation of multi-scale modelling is first explored after which a benchmark model representing one section of the LHC tunnel is built. The model contains one 640m long 3D domain, accommodating a 1MW fire, while the remainder of the domain is made up out of 1D ducts. Special attention is paid to the correct implementation of the push-pull ventilation strategy and selection of the 3D domain size. Following the construction of the benchmark system, it is subjected to a number of sensitivity analyses focussing on both the 1D and 3D portions of the domain. The development of the flow is investigated based on the Froude number and the temperature and velocity profiles of the flow along the tunnel. As such it is shown that the condition Fr_{ing}=3.2 serves as a sufficient but not necessary condition in determining the length of the 3D downstream domain. By suggesting possible improvements to the multi-scale model, the door is opened to future research.

Fire Safety Engineering
Lund University
P.O. Box 118
SE-221 00 Lund
Sweden

http://www.brand.lth.se

Telephone: +46 46 222 73 60

HOST UNIVERSITY: Lund University

FACULTY: LTH

DEPARTMENT: Division of Fire Safety Engineering

Academic Year 2017-2018

Multi-scale modelling of fire in accelerator tunnels: a CERN case study

Melchior Schepers

Promoter: Prof. PhD ir. Ing. Patrick van Hees
Co-promoter: Jonathan Wahlqvist

Master thesis submitted in the Erasmus Mundus Study Programme

International Master of Science in Fire Safety Engineering

DISCLAIMER

This thesis is submitted in partial fulfilment of the requirements for the degree of *The International Master of Science in Fire Safety Engineering (IMFSE)*. This thesis has never been submitted for any degree or examination to any other University/programme. The author(s) declare(s) that this thesis is original work except where stated. This declaration constitutes an assertion that full and accurate references and citations have been included for all material, directly included and indirectly contributing to the thesis. The author(s) gives (give) permission to make this master thesis available for consultation and to copy parts of this master thesis for personal use. In the case of any other use, the limitations of the copyright have to be respected, in particular with regard to the obligation to state expressly the source when quoting results from this master thesis. The thesis supervisor must be informed when data or results are used.

Melchior Schepers

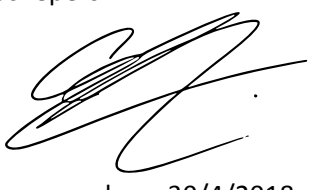

Read and approved 30/4/2018

Preface

I was granted the amazing opportunity to not only perform this thesis in cooporation with perhaps the most sophisticated research institute in the world, CERN, but to also visit it. The level of sophistication and engineering involved in running the world's largest particle accelerator is truly awe-inducing.

A thesis cannot be complete without a word of thanks. Over the course of the last few months I have come to learn that this is not just a moment of obligatory praise, but a true and sincere moment of reflection. A moment of reflection on all the people without whom this dissertation would not have been possible.

I owe a great deal of gratitude to professor Patrick van Hees for the amount of flexibility he demonstrated and the assistance he provided during the duration of this thesis. I also want to thank Oriol Rios who helped me get my facts straight and to whom I could always turn for help. Jonathan Wahlqvist also needs mentioning for his feedback and help with any FDS quirks. A sincere thank you is finally also needed to Saverio La Mendola and CERN for making this collaboration possible and providing me with this interesting topic.

This thesis marks the end of my IMFSE experience and my academic education as an engineer as a whole. The last few years have been an incredible journey. However I would not have gotten to this point if it were not for the support of my family and girlfriend, Laura. Last but definitely not least I want to thank my aunt and uncle for their financial support in making this master possible. Monique, Jul, ***Thank you!***

"Knowledge always desires increase; it is like fire, which must first be kindled by some external agent, but which will afterwards propagate itself."
Samuel Johnson

Melchior Schepers

Abstract

Multi-scale modelling is a novel approach to fire modelling in situations where the size of the domain prevents it from being modelled completely in 3D. By splitting the domain in a 1D and 3D portion multi-scale modelling allows for much faster simulations which still adhere to the correct boundary conditions. In this thesis the multi-scale methodology is applied to the LHC accelerator in use at CERN using the HVAC capabilities of FDS. The theoretical foundation of multi-scale modelling is first explored after which a benchmark model representing one section of the LHC tunnel is built. The model contains one 640m long 3D domain, accommodating a 1MW fire, while the remainder of the domain is made up out of 1D ducts. Special attention is paid to the correct implementation of the push-pull ventilation strategy and selection of the 3D domain size. Following the construction of the benchmark system, it is subjected to a number of sensitivity analyses focussing on both the 1D and 3D portions of the domain. The development of the flow is investigated based on the Froude number and the temperature and velocity profiles of the flow along the tunnel. As such it is shown that the condition $Fr_{ing} = 3.2$ serves as a sufficient but not necessary condition in determining the length of the 3D downstream domain. By suggesting possible improvements to the multi-scale model, the door is opened to future research.

Multi-scale modellering is een nieuwe benadering in het modelleren van rook en brand in systemen waarbij de grootte van het domein een meer conventionele volledige 3D modellering onmogelijk maakt. Het domein wordt opgesplitst in een 1D en 3D gedeelte om zo de simulatietijd te verminderen. In deze thesis wordt de multi-scale methodologie toegepast op de LHC deeltjesversneller te CERN met behulp van de HVAC module van FDS. Eerst wordt de theoretische basis van multi-scale modellering uitgelegd, alvorens over te gaan tot het modelleren van één sectie van de LHC tunnel. Het gebouwde referentiemodel omvat in totaal 3km aan tunnel, waarvan 640m in 3D, waarin zich een 1MW brand bevindt. Het overige gedeelte bestaat uit een 1D netwerkmodel. Specifieke aandacht wordt besteed aan de implementatie van de correcte ventilatie-randvoorwaarden en de keuze van het 3D domein. Het geconstrueerde referentiesysteem wordt vervolgens onderworpen aan een reeks gevoeligheidsanalyses, die zowel betrekking hebben op het 1D als 3D gedeelte van het model. De ontwikkeling van de stroming wordt geanalyseerd op basis van zowel het Froudegetal als van het temperatuurs- en snelheidsprofiel van de stroming doorheen de tunnel. Dusdanig wordt aangetoond dat $Fr_{ing} = 3.2$ een voldoende maar niet noodzakelijke voorwaarde is voor de bepaling van de lengte van het 3D domein. Suggesties voor mogelijk bijkomend onderzoek vormen het sluitstuk van deze thesis.

Contents

List of Figures and Tables

List of Figures

List of Tables

List of abbreviations and symbols

Abbreviations

3D	three-dimensional
ALICE	A Large Ion Collider Experiment
ATLAS	A Toroidal LHC AppartuS
BEH	Brout Englert Higgs
CERN	Conseil Européen pour la Recherche Nucléaire - European Organization for Nuclear Research
CFD	computational fluid dynamics
CMS	Compact Muon Solenoid
DNS	direct numerical simulation
FCC	Future Circular Collider
FDS	Fire Dynamics Simulator
FFT	Fast Fourier Transform
HPC	high performance computing
HRR	heat release rate
HVAC	heating, ventilation and air conditioning
LEP	Large Electron Positron
LES	large eddy simulation
LHC	Large Hadron Collider
LHCb	Large Hadron Collider beauty
Linac 2	Linear Accelerator 2
MPI	message passing interface
MP	multi processing
NIST	National Institute of Standards and Technology
NS	Navier-Stokes
PS	Proton Synchrotron
RANS	Reynolds averaged Navier Stokes
RPM	rotations per minute
SGS	subgrid scale

Symbols

a	radius	$[m]$
A	duct cross section	$[m^2]$
c_p	specific heat capacity	$[J/(kgK)]$
D^*	characteristic length scale of fire	$[m]$
D_h	hydraulic diameter	$[m]$
f	Darcy friction factor	$[-]$
Fr	Froude Number	$[-]$
g	standard acceleration due to gravity	$[m/s^2]$
h	enthalpy or convective heat transfer coefficient	$[J]$ or $[W/(m^2K)]$
H	tunnel height	$[m]$
k	thermal conductivity	$[W/(mK)]$
K	dimensionless loss coefficient	$[-]$
L	duct length	$[m]$
L_b	back-layering length	$[m]$
L_b^*	non-dimensional back-layering length	$[-]$
Nu	Nusselt number	$[-]$
P	perimeter	$[m]$
Pr	Prandtl number	$[-]$
p	pressure	$[Pa]$
Δp	pressure difference	$[Pa]$
$\dot{q}'''$	volumetric heat production rate	$[W/m^3]$
$\dot{Q}$	HRR	$[W]$
$\dot{Q}^*$	non-dimensional HRR	$[-]$
Re	Reynolds Number	$[-]$
T	Temperature	$[K]$
ΔT	temperature difference	$[K]$
u	duct velocity or x-component of velocity vector	$[m/s]$
u^*	non-dimensional x-component of velocity vector	$[-]$
$\dot{V}$	volumetric flow rate	$[m^3/s]$
V	volume	$[m^3]$
δx	mesh cell dimension in x-direction	$[m]$
δy	mesh cell dimension in y-direction	$[m]$
z	height	$[m]$
Δz	height difference	$[m]$
δz	mesh cell dimension in z-direction	$[m]$
	Vectors	
$\mathbf{f}$	body force vector	$[N/m^3]$
$\mathbf{q''}$	heat flux per unit area	$[W/m^2]$
$\boldsymbol{\tau}$	deviatoric stress tensor	$[Pa]$
$\mathbf{v}$	velocity vector	$[m/s]$

	Greek letters	
α	thermal diffusivity	$[m^2/s]$
Δ	LES filter width	$[m]$
ϵ	absolute surface roughness	$[m]$
μ	dynamic viscosity	$[Pas]$
ν	kinematic viscosity	$[m^2/s]$
ρ	density	$[kg/m^3]$

Chapter 1

Introduction, objectives & methodology

Fire safety is an often overlooked part of infrastructure design. The measures needed to ensure a fire safe environment are often costly and the chances of a fire occurring usually slim. This unbalance between cost and occurrence often tips the scale towards budget cuts on fire safety expenses. A proper fire safety policy can however save lives and property if taken into account from the onset of a project.
In order to mitigate the effects of a fire, appropriate safety measures are needed. Implementing these measures, however requires a thorough understanding of the way in which a fire will develop and interact with its surrounding. Thus creating the need for accurate modelling of fire.
Fire safety engineering is a relatively new discipline compared to the more conventional engineering disciplines such as mechanical and civil engineering, but has gained more and more traction over the last few decades. Nevertheless there are still many advancements to be made. This is especially true in the field of fire modelling, which relies on the solution of the Navier-Stokes equations. To this day these are still impossible to solve directly for practical situations. The main bottleneck is the available computational power and thus other techniques such as multi-scale modelling provide the best option for accurate modelling at this point. Multi-scale modelling combines the strengths and weaknesses of both 3D and 1D modelling. By joining them into one model, the detail provided by 3D modelling is combined with the computational speed of 1D modelling.

1.1 Problem statement

The complexity and scale of the particle accelerator tunnels at the site of the European Organization for Nuclear research (CERN) prevent them from being completely modelled by 3D computational fluid dynamics (CFD). The Large Hadron Collider (LHC) is 27km long and the yet-to-be-built Future Circular Collider (FCC) is potentially even 100km long. Trying to simulate such domains with a purely 3D CFD approach would lead to infeasible amounts of computing power needed, to come

up with a result in a reasonable time span. Other options thus have to be explored in order to model smoke movement and fire behaviour in (accelerator) tunnels. In this dissertation multi-scale modelling will be the prime instrument used to get an idea of the conditions in large particle accelerator tunnels caused by a fire.
The characteristics of accelerator tunnels provide for specific difficulties in modelling of the tunnel. There is no direct connection to ambient conditions as with a conventional tunnel and in the LHC currently a longitudinal push-pull ventilation system is used, which has not been modelled using a multi-scale approach before. The main objective of this thesis can thus be summarised to be: *"Investigate the feasibility of multi-scale modelling of fires in the underground particle accelerators being used at CERN."*. This includes:

- Researching the implementation and capabilities of multi-scale modelling within the Fire Dynamics Simulator (FDS).
- Developing a correct representation of the tunnel system at CERN, which can serve as a benchmark for further research. This starts by developing a realistic representation of the ventilation system and tunnel geometry and is concluded by the selection of a suitable cell size.
- Investigating the assumptions made in the development of the benchmark system and its sensitivity to both 1D and 3D parameters.
- Researching how the flow develops inside the 3D model and evaluating which parameters act as indicators for determining the 3D domain length.

1.2 Methodology

The methodology followed in this thesis starts from a blank canvas. Meaning that the entire chain from theoretical background until practical implementation of multi-scale modelling in FDS is followed. The coming paragraphs explain how the different chapters follow this roadmap and what the resources are that will be used to bring this quest to a successful conclusion.

1.2.1 Thesis roadmap

After a general introduction on fire safety in the first chapter, the theoretical foundation of multi-scale modelling is laid out in chapter two. It handles both standard 3D modelling techniques such as Reynolds Averaged Navier-Stokes (RANS) and Large Eddy Simulation (LES) as well as 1D modelling. Once the theoretical foundation is in place the already performed research is reviewed.
Chapter three is dedicated to getting to grips with the LHC the main accelerator in use at CERN today. It provides information on usage, layout and the ventilation system in use. The final sections are dedicated to development of plausible fire scenarios and the introduction of an FDS design fire.
Chapter four develops a reference case, to act as a benchmark system in the remainder

of this thesis but also in research to come. The case is built from the ground up. starting with the implementation of the ventilation system and tunnel shape, after which the 3D and 1D domains are specified and finally a suitable mesh is selected. The fifth chapter addresses the assumptions made in the design of the benchmark system and subjects it to multiple sensitivity analyses addressing both 1D and 3D parameters. The final chapter summarises the main conclusions and suggests possible improvements to the benchmark system.

1.2.2 Resources

The general work flow of the simulations performed in this dissertation can be summarised as:

$$Building\ the\ FDS\ source\ code \Longrightarrow Running\ the\ simulation \Longrightarrow Post-processing\ of\ the\ results$$

This highlights three important steps, each with their own specific resources both in terms of software as hardware and which are covered below.

Building the source code: FDS

The main software used in this thesis for modelling purposes is FDS. FDS is a computational fluid dynamics package, mainly developed by the National Institute of Standards and Technology (NIST). It is widely used throughout the fire safety engineering community. The first version was publicly released in February 2000 [21]. At the time of writing, release 6.7.0 is in preparation. In this thesis version 6.5.3 is used, since this is the version installed on the computational cluster at CERN, on which the simulations were run.
FDS provides a numerical approach to solving a simplified form of the Navier-Stokes equations based on a large eddy simulation technique. It is a very powerful tool to address fire phenomena, but it should always be kept in mind that the results are based on a large number of assumptions and an idealisation of reality. The results should thus always be met with a critical view.
Multi-scale modelling is made available in FDS by usage of the HVAC module. This module allows to couple 1D elements to the 3D domain. Although originally intended purely to model the behaviour of heat and combustion products throughout a HVAC duct network, it can also be used for multi-scale modelling. A more detailed explanation of the HVAC capabilities is given in chapter 2.

The FDS source file is constructed using a simple text editor but also Pyrosim was used for modelling purposes. Pyrosim provides a graphical user interface in order to construct the FDS source file and is a handy tool to visually check the FDS code.

Running the simulation: The CERN HPC-cluster

Once the FDS source files are constructed the simulations can be started. Thanks to the cooperation with CERN, it was possible to run all simulations in this thesis on the CERN HPC-cluster. This cluster runs on CentOS Linux 7.4, employing OpenMPI and MVAPICH 2.2. The available nodes are split into BATCH and BE nodes. The BATCH nodes are Transtech Quad HPC servers with 16 cores and 128 Gb of memory. They utilise 10Gb low latency Ethernet cards (Chelsio T520-LL-CR) and Intel Xeon E5-2650 v2 processors running at 2.60GHz.
The BE nodes are Format Quad servers with 20 cores and 128GB of DDR4 memory. The CPU's are Intel Xeon E5-2630 v4 running at 2.20GHz, connected through Mellanox FDR InfiniBand switches. Appendix C contains a complete list of every simulation discussed in this thesis with its computational characteristics.
The downside of running the simulations on the CERN servers is that all output files had to be downloaded from the cloud. This makes adding slice files to the 3D domain virtually impossible due to the size of these output files. All results were therefore output using DEVC devices in FDS. This has the added benefit that also the conditions within the 1D ducts could be monitored since these are not available through slice files.

Post-processing the results: Matlab and Smokeview

Post processing of the results is done using both Matlab and Smokeview. Matlab is used to import the .csv file output by the FDS devices and to graphically plot the results. It is also used to easily calculate the Froude number. The Matlab code developed for this purpose is included in appendix A. Smokeview on the other hand is the standard tool developed by NIST to visualize FDS simulation data. It allows to monitor smoke movement within the 3D domain and as such provides easy access to visual verification of back-layering length and smoke positions at different points in time.

1.3 Fire safety in tunnels

Over the last few decades multiple incidents in tunnels have made news headlines worldwide. Both in road and railway tunnels catastrophic events have occurred. The most notable fires include: the Mont Blanc Tunnel fire in 1999, the Kaprun skitrain disaster in 2000 and a fire in 2003 in a South Korean metro tunnel killing more than 200 people [2].
A fire taking place in a tunnel is often more devastating than the same fire occurring in the open. The confined nature enforces heat feedback to the fire source and makes it hard for rescue services to reach the seat of the fire and for occupants to escape.

In recent years tunnel fire safety has followed the general trend in the fire safety community of moving from a prescriptive approach towards a performance-based approach [2]. With this shift also comes the need for better modelling techniques,

which serve as the foundation of performance-based decision making. One of those techniques is multi-scale modelling. Certainly at CERN the need for accurate models is a must, since their installations fall outside the scope of any regulations.
But not only the modelling techniques need to be improved, also the mitigation measures taken in tunnels are under continuous development. One of the most important mitigation measures is a tunnel's ventilation system. It plays a crucial role in how combustion gasses and smoke particles will spread throughout the tunnel. The following section will provide an overview of the most common ventilation systems in tunnels.

1.4 Tunnel ventilation

Ventilation systems in tunnels were originally developed to dilute the concentration of dangerous gasses and heat resulting from internal combustion engines in road and railway tunnels. Over the years ventilation systems have however evolved from a purely practical role to being the main mitigation system in case of fire [15]. There are two main groups of ventilation systems, namely natural systems and mechanically powered systems.

1.4.1 Natural ventilation

Natural ventilation systems rely on external factors to ensure the movement of air inside a tunnel. This can be the piston effect caused by a moving train for railway tunnels or the existence of a pressure difference between tunnel portals due to a height difference. The simplicity of natural systems, makes them cheap to employ but is also their Achilles heel as they are dependent on external factors such as meteorological conditions at the portals of the tunnel.
Natural ventilation can only be employed in tunnels up to 400-500m as this is the distance over which the smoke stratification of a fire can be maintained [2]. The hot plume rises towards the ceiling and spreads out radially, moving towards the tunnel portals. Underneath this hot layer there is an inflow of cold ambient air. It is argued that this cold region can allow for a safe passage of tunnel occupants [2]. With increasing length the hot upper layer is however quickly eroded due to heat transfer towards the walls and turbulent mixing at the interface with the cold bottom layer [2]. The hot smoke and cold air mix and the buoyancy succumbs to gravity. Both turbulent mixing and heat transfer to the walls are proportional to the length travelled by the upper layer and as a result limit the feasible length of a naturally ventilated tunnel [2].

1.4.2 Mechanical ventilation

As opposed to naturally ventilated tunnels, mechanically ventilated tunnels use a powered fan or exhaust system to ensure a safe passage in case of fire and to dilute pollutants. They are the most used ventilation system today and are typically

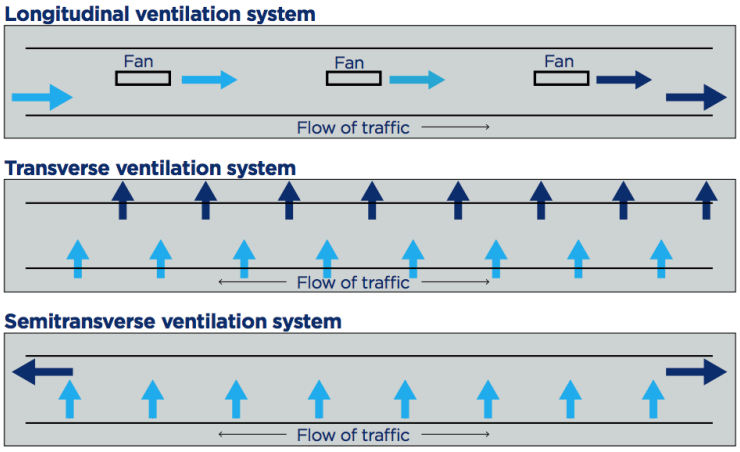

Figure 1.1: The different mechanical ventilation systems [27]

used in longer tunnels ensuring a higher level of safety than would be attainable with a natural system [15]. Mechanical ventilation systems can be subdivided in the following categories: longitudinal, transverse and semi-transverse. Their basic lay-out is shown in figure 1.1.

Longitudinal ventilation

Longitudinal systems create a longitudinal flow of air. The tunnel bore acts as a large duct, eliminating the need for additional ductwork. This makes this type of ventilation system relatively cheap to implement. The longitudinal airflow can be created by using jet fans, by injecting air into the middle of the tunnel or by using a push-pull type of system as illustrated in figure 1.2. It is such a push-pull system that is currently in use in the LHC accelerator at CERN.

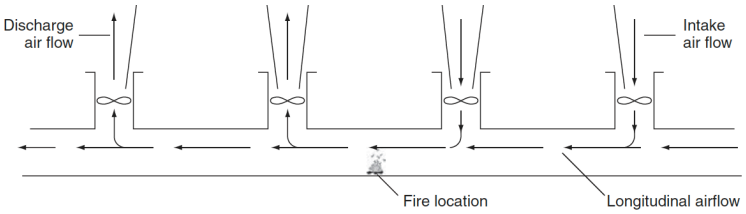

Figure 1.2: longitudinal push-pull configuration [2]

A lot of the research around longitudinal ventilation has focussed on preventing back-layering. To avoid smoke moving upstream of the fire a critical airspeed has to be achieved [15]. The idea behind this is that people downstream of the fire can escape in the direction of traffic, while the people upstream of the fire have a

smoke-free path to evacuate. The critical velocity is dependent on both the HRR and geometry of the tunnel. A value of $3\,m/s$ typically suffices to prevent back-layering.

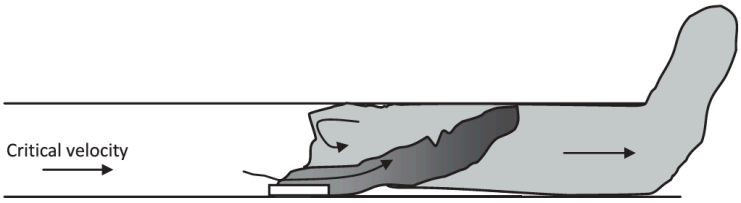

Figure 1.3: Prevention of back-layering by ensuring the airflow maintains the critical velocity [15]

Transverse ventilation

In a transverse ventilation system the airflow is directed perpendicular to the cross section of the tunnel. Extraction usually happens at the top, while the supply originates at the bottom [15]. A transverse system has the benefit that pollutants and smoke can be extracted almost immediately at their point of origin, creating a smoke-free environment in the proximity of the fire. This facilitates fire fighter intervention and evacuation of occupants. The main disadvantage of a transverse system is the complexity and cost to implement it along a long tunnel. Additional ductwork or even an extra tunnel bore is necessary to extract dangerous gasses and supply fresh air throughout the tunnel.

Semi-transverse ventilation

A semi-transverse system is similar to a fully transverse ventilation system, but rather than equipping the tunnel with both an exhaust and inlet duct only one of the two is provided. Semi-transverse set-ups can be subdivided into:

- A *supply air semi-transverse system* only foresees in a duct for the supply of fresh air. Contaminated air is pushed out through the portals. In a fire situation it is however necessary to have an inflow of fresh air through the portals in order to facilitate fire fighter intervention. Thus it has to be possible to reverse the operation of the system in case of an emergency [2].
- An *exhaust semi-transverse system* only provides extraction of vitiated air. Fresh air is drawn into the tunnel via shafts or via the portals.

Modern systems often employ combinations of the techniques discussed above, making it hard to categorize them as strictly longitudinal, transverse or semi-transverse systems. These so called combined systems incorporate the advantages of each type in order to provide the most efficient solution to a specific case.

Chapter 2

Multi-scale modelling

The complexity and scale of the particle accelerator tunnels at the CERN site prevent them from being completely modelled by 3D CFD. The LHC is 27km long and the yet-to-be-built FCC is potentially even 100km long. The turbulent scales of motion from the fire on the other hand range down to millimeters. The relevant length scales, which would have to be resolved thus span orders of magnitude around $10^7 - 10^8$. The size of the mesh that would be needed to model the domain of such a tunnel with enough detail would result in unrealistic simulation times. This makes multi-scale modelling at this point the only feasible modelling technique. The enormity of the tunnels, does however also pose difficulties for multi-scale modelling in that only a small part of the domain can be modelled using 3D CFD. This poses difficulties in correctly defining the boundary conditions of the 3D domain, certainly in the LHC tunnel, where no compartmentalization is present.

2.1 Multi-scale modelling: the concept

Multi-scale modelling of ventilation systems in tunnels is a novel technique that is computationally much more favourable than a complete 3D CFD calculation. It is based on the combination of 1D and 3D CFD modelling techniques.
By using a multi-scale approach the computational domain is physically decoupled into a near field surrounding the fire and a simplified far field further from the fire, where the flow is fully developed [12]. The near field is modelled using 3D CFD, which can be based on a RANS-approach, a LES-approach or other approximation procedures. The far field is modelled by a computationally much more favourable 1D network approach, based on graph theory [12]. An example of such a decomposition is shown in figure 2.1. On the one hand the coupling between the near field and far field allows for accurate and computationally fast results. On the other hand this coupling also brings with it specific difficulties. These will be addressed later on.

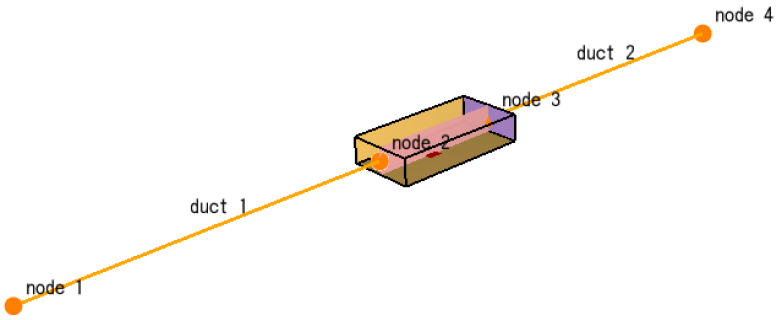

Figure 2.1: Nodes and branches (ducts) connected to a 3D domain

2.1.1 3D CFD

Computational fluid dynamics uses discretization techniques to approximate the Navier-Stokes equations, which govern the motion of fluids. In the case of FDS a second-order accurate finite difference method is applied to perform the discretization [20]. The Navier-Stokes equation as given by equation (2.1) expresses the conservation of momentum for a fluid.

$$\rho \frac{D\mathbf{v}}{Dt} = -\nabla p + \nabla \cdot \boldsymbol{\tau} + \mathbf{f} \tag{2.1}$$

In its most general form equation (2.1) cannot be solved. Extra assumptions have to be made concerning the type of fluid (e.g. Newtonian) and thermodynamic equations of state, relating temperature, density and pressure [24]. Together with the continuity equation (2.2) and energy equation (2.3) this results in a set of coupled non-linear partial differential equations describing the motion of a fluid.

$$\frac{d\rho}{dt} + \nabla \cdot (\rho \mathbf{v}) = 0 \tag{2.2}$$

$$\rho \frac{Dh}{Dt} = \frac{dp}{dt} + \boldsymbol{\tau} : \nabla \mathbf{v} - \nabla \cdot \mathbf{q}'' + \dot{q}''' \tag{2.3}$$

The equations as given above describe all fluid flow phenomena. They contain an enormous amount of detail, much of which can be omitted when describing fire phenomena [20]. Simplifying the equations, greatly enhances the computational efficiency, without endangering the validity of the solution. The simplified equations used throughout much of the fire science community were first derived by Rehm and Baum [25] and are commonly referred to as the "low Mach number combustion equations". They model the movement of slow moving gasses driven by chemical heat release and buoyancy forces [20]. At low speeds the fluid can be assumed to be incompressible and this assumption allows the energy equation to be decoupled from the momentum and continuity equation, simplifying the solution. Yet even simplified, analytical solutions for the equations do not exist and engineers and

scientists have to resort to numerical simulation. There are several approaches to solving the Navier-Stokes equations numerically, but the two most commonly used are RANS and LES.

Reynolds averaged Navier-Stokes

Reynolds averaged Navier-Stokes, commonly known as RANS can be seen as a time averaged or low-pass filtered version of the NS-equations. This observation stems from the fact that the variables can be represented by their time average and a perturbation around this average, by using Reynolds decomposition. Doing so, results in extra unknowns being introduced into the set of equations. These unknowns are referred to as the Reynolds stresses and constitute the basis of the "turbulence closure problem" [19]. That is: the averaging leads to more unknowns than equations. In order to overcome this problem empirical models have to be introduced. One such model is the $k\epsilon - model$, which is in widespread use today.
A major shortcoming of the RANS-approach results from the time-averaging itself. The results are smeared out in time, making them unsuitable for modelling the short time/small length scale interactions between turbulence and other short time frame phenomena such as combustion [19]. All scales of motion, from the integral scale down to the dissipation range are modelled in a RANS-approach. Only mean values are calculated directly [19]. This means that even with decreasing grid size, a RANS-approach will never give an exact solution to the NS-equations. Only with an exact representation of the Reynolds stresses an exact solution to the time averaged NS-equations can be obtained. The exact formulation of the Reynold stresses can however only be achieved through direct numerical simulation (DNS) [19].

Large eddy simulation

Rather than a temporal filter, large eddy simulation or LES can be considered as spatially filtering the NS-equations. This might suggest an analogy between RANS and LES, but the two methods are vastly different. Whereas the Reynolds decomposition effectively removes the time dependence of the solution, the LES decomposition retains the time dependence of both the resolved and the modelled part and is able to deliver a time-dependent solution [19].
LES is the standard mode of operation of FDS. The NS-equations are filtered using a spatial low-pass filter with width $\Delta = V_c^{1/3} = (\delta x \delta y \delta z)^{1/3}$. Here $\delta x,\ \delta y$ and δz are the dimensions of the mesh cells [20]. The turbulent phenomena with a characteristic length scale larger than the filter width are resolved, while the ones with a length scale smaller than the filter width are modelled. The modelling is once again a direct consequence of the filtering operation and the afore-mentioned closure problem. The modelled stresses are referred to as the subgrid scale (SGS) stresses [20]. To model these FDS uses the Deardorff model [13] by default.
In FDS the filter width is a direct function of the cell size. This means that also the accuracy of the result is a function of the cell size. In the limit of a cell size going towards zero an LES-simulation should converge to the result of a DNS. Decreasing

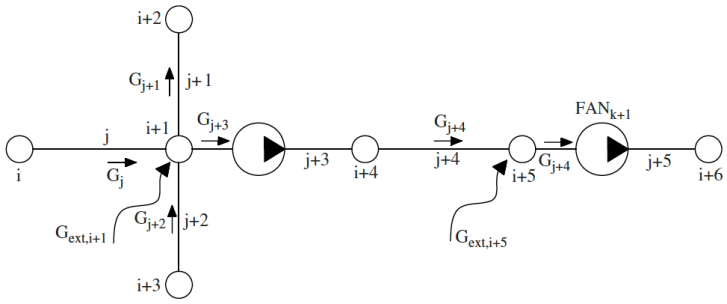

Figure 2.2: Example of a network model[8]

the cell size however comes at a price as increasing the number of cells also means increasing the computational time. The question thus arises what an acceptable mesh resolution is. Guidance is given by the pope criterion [23]. Pope defines LES for the canonical case of isotropic turbulence such that at least 80% of the kinetic energy should be resolved [21]. In other words: at most 20% of the kinetic energy of the flow field should be contained in the subgrid scales of motion.
The main disadvantage of LES over RANS is the increased computational time. It can be shown that the total arithmetic needed to complete a RANS simulation is a weak function of the Reynolds Number, $\mathcal{O}(Re)$ [19]. LES on the other hand is $\mathcal{O}(Re^2)$, and DNS is $\mathcal{O}(Re^3)$, thus explaining the drastic increase in computational time from RANS →LES →DNS [19]. LES is currently the state of the art and as explained above, from a formal mathematical point of view also a more correct approach to solving the NS-equations. With decreasing grid size it converges to DNS, which is currently impossible except for the simplest of problems. In a sense LES can be seen as a form of multi-scale modelling. The region of interest is modelled with greatest accuracy and the smaller scales are approached using simpler modelling methods.

2.1.2 Network modelling

It was highlighted in the previous section that 3D CFD, and specifically LES is a costly operation to perform from a computational point of view. To reduce the total arithmetic needed for a simulation, in a multi-scale model part of the domain is modelled by a 1D network model. Network modelling is based on graph theory and represents the domain as a connection of branches and nodes as displayed in figure 2.2. The assumption is made that there is no variation in fluid properties across the cross section of the tunnel, but only in the longitudinal direction. There is no more stratification of the smoke and the flow is well-mixed. Starting from this region onwards, the flow can be modelled by a 1D network. The 1D network allows to solve a much more simplified form of the Navier-Stokes equations, with the equations for conservation of mass and momentum now being able to be expressed in 1D. Computationally this is a much more favourable operation to perform since it allows for much faster solution procedures.

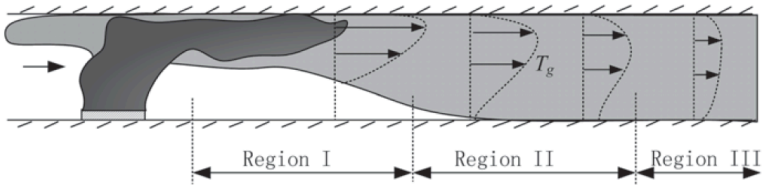

Figure 2.3: Flow development with longitudinal ventilation [15]

2.1.3 Coupling 1D and 3D CFD

There are two ways of coupling the 3D domain with the 1D domain. A direct or an indirect coupling method. In the former the equations for the 1D model and 3D model are solved simultaneously, while in the latter first the 3D model is solved for after which the 1D model can quickly be calculated. In FDS an indirect coupling procedure is used, as will be explained in the next section 2.2.
Equally important as the coupling method itself is the location of the coupling. It was highlighted in the previous paragraph 2.1.2 that the 1D network assumes that there is no gradient over the height of the tunnel for any of the flow properties. The interface between the 1D and 3D region should thus be placed at a position no sooner than that the flow has become fully developed. This identifies one of the main difficulties in building an accurate multi-scale model: from which point onwards can the flow be considered fully developed? A possible indicator is the local Froude number. Both Newman and Ingason have looked at smoke stratification in tunnels using the Froude number and have tried to identify different regions with different degrees of stratification as explained below.

Smoke regions

Newman [22] and Ingason [15], identified three stratification regions based on the local Froude Number. The first region is characterised by strong stratification and occurs for $Fr \leq 0.9$. $0.9 \leq Fr \leq 3.2$[1] bounds the second region and is a mixing zone for hot smoke and cold ambient air. The third region is identified by $Fr > 3.2$ and represents the fully developed zone [15]. Figure 2.3 shows the different stratification zones and shows that it is not until region III (figure 2.3) that the flow becomes well-mixed with only marginal transversal gradients. The inequality $Fr > 3.2$ can thus act as an indication for the location of the interface between the two domains. Colella et al. [9] furthermore showed that the distance of the downstream boundary of the 3D domain to the fire source should at least be thirteen times the hydraulic diameter of the tunnel. This leads to two criteria, which can be checked in order to decide on the boundary interface location. These conditions are later verified and the position of the boundary interface will also be subject to a sensitivity study later on in this work.

[1] Newman originally used a value of 10 to indicate the fully developed region, but here the value of 3.2 defined by Ingason is used.

2.2 Multi-scale modelling in FDS

In FDS network modelling is made available by usage of the HVAC functionality. The HVAC network consists of a set of nodes connected by ducts. In each node, the conservation equations for mass (2.4), energy (2.5) and momentum (2.6) are solved [20]. Note that these are the same governing equations expressed in 1D (and with simplifications) as were discussed in section 2.1.1 in vector format. The subscripts $_j$ represent the duct segments, while the subscripts $_i$ and $_k$ refer to nodes. The equations for mass and energy are solved using an explicit solver, the momentum equation is solved implicitly [20].

$$\sum_j \rho_j u_j A_j = 0 \tag{2.4}$$

$$\sum_j \rho_j u_j A_j h_j = 0 \tag{2.5}$$

$$\rho_j L_j \frac{du_j}{dt} = (p_i - p_k) + (\rho g \Delta z)_j + \Delta p_j - \frac{1}{2} K_j \rho_j |u_j| u_j \tag{2.6}$$

To couple this system of equations with the 3D domain an indirect coupling method is used in FDS, the procedure of which is outlined in figure 2.4. First the 3D domain is solved for after which the values at the interface position are averaged and serve as boundary conditions for the 1D solver. The HVAC solver is then called and used to update the 3D boundary conditions. This loop continues until the simulation reaches a numerical instability or the specified end time.

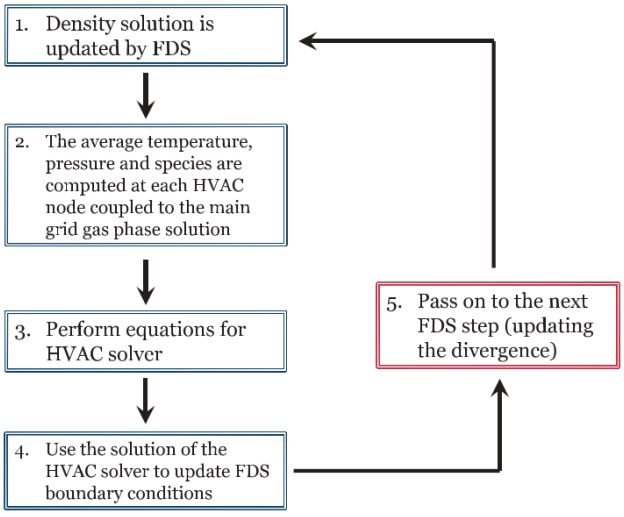

Figure 2.4: The indirect coupling procedure followed in FDS [29]

2.2.1 Limitations of multi-scale modelling in FDS

It is important to note that the HVAC feature in FDS was not developed with multi-scale modelling of tunnel networks in mind, but rather to provide a tool to model the flow of heat and combustion products through HVAC networks [21]. Using HVAC networks to represent the 1D network of a large multi-scale model is thus not a well-supported feature of the software, making it prone to numerical instabilities and errors. In the following, the main pitfalls and shortcomings are listed.

The absence of heat transfer in HVAC ducts

A major flaw in using multi-scale modelling in FDS stems from the fact that heat loss is not included in the 1D network. Cosentino [12] tried to overcome this by modifying the source code of FDS, but to this point these changes have not yet been implemented in the latest release of FDS 6.6.0. A possible work around to this problem is provided by the possibility to include heat exchangers or so-called aircoils in FDS. The theoretical foundation for this workaround is provided here, but it is left as a suggestion to future research to investigate the feasibility of this solution in practice.

In the analysis that follows, the influence of radiation is ignored. This is based on the assumption that the 3D-1D interface is taken far enough from the fire, the dominant heat transfer process can then be assumed to be convection. The heat loss to the environment can now be calculated using empirical relations based on the Nusselt number. To do so the following step by step process can be followed [28]:

1. Determine the average fluid temperature at the end of the 3D domain right before the downstream interface: T_f^*.

2. Evaluate the fluid properties[2] at the determined temperature T_f^*. Namely: thermal conductivity k, dynamic viscosity μ, density ρ and specific heat capacity c_p.

3. Calculate the kinematic viscosity $\nu = \frac{\mu}{\rho}$ and thermal diffusivity $\alpha = \frac{k}{\rho \cdot c_p}$.

4. Calculate the Prandtl number, $Pr = \frac{\nu}{\alpha}$ and the Reynolds number, $Re = \frac{u \cdot D_h}{\nu}$.

5. Determine the Darcy friction factor f[3] by employing the Colebrook and White equation:

$$\frac{1}{\sqrt{f}} = 3.48 - 1.7373\ ln\left(\frac{\epsilon}{a} + \frac{9.35}{Re \cdot \sqrt{f}}\right) \qquad 4 \cdot 10^3 \leq Re \leq 10^8$$

   With ϵ the surface roughness and a the radius of the pipe.

[2] e.g. using thermodynamic tables

[3] The assumption is that the flow is through a rough pipe

6. Calculate the Nusselt number by using an empirical correlation such as the one by Kawase and Ulbrecht:

$$Nu = 0.0523 Re Pr^{1/2} \sqrt{f}$$

7. Determine the convective heat transfer coefficient $h = \frac{Nu \cdot k}{D_h}$

By splitting the 1D ducts in multiple sections of e.g. 50m the heat loss in every section can then be estimated. Assuming the tunnel acts as an infinite heat sink, the wall temperature can be assumed constant at ambient conditions of 293K. The heat loss to the walls in the first section can now be determined as $\dot{Q} = hA(T_{wall} - T_f^*)$, which can be implemented by using a FIXED_Q aircoil in FDS. The temperature T_f^* can then be measured at the downstream node of the first section and the process can be repeated until an aircoil is associated with every duct, or the temperature of the fluid reaches ambient conditions.

The absence of fan control

FDS is a fluid dynamics package, and was not developed for purposes of control theory. The implementation of a fan is only possible via definition of one fan curve, while in reality it is common practice to control the fan within a certain RPM operating range. The only control possible within FDS is switching a fan on or off. A problem related to this, is the "non-localised" problem which is elaborated upon and for which a workaround is provided in section 4.2.1.

Mass storage

Mass storage in the 1D network is not activated by default, but can be turned on by specifying HVAC_MASS_TRANSPORT=.TRUE. on the &MISC line [21]. However it was noted that this greatly enhanced the instability of the simulations and was not set to true in this thesis.

2.3 Literature review

In comparison to well-established engineering disciplines such as mechanical or civil engineering, fire safety engineering is a relatively new field of study. Multi-scale modelling is a novel subject even within this field and so the performed research within this niche can be traced back to just a handful of authors.
While the idea of multi-scale modelling was not new, Colella was the first to explore the concept for fire modelling in his PhD thesis [7]. In his thesis he proved that it was a feasible option to model a traffic tunnel in fire conditions using a RANS approach in ANSYS FLUENT. The results obtained via the simulations were validated using the results of the Dartford tunnel experiments. The research of Colella et al. was published in multiple papers [8], [10], [9], [11].
In turn Vermesi proved in her master thesis that multi-scale modelling is also a viable

option in FDS using the HVAC capabilities and a LES approach [30]. The results of the research of Vermesi et al. was later also published in an article [29], exploring the multi-scale modelling capabilities of FDS.
In 2015 Ang et al. published the results of their multi-scale FDS simulations, replicating the Dartford tunnel experiments [1]. Their research showed that the FDS multi-scale approach was able to withstand experimental validation in simple road tunnels, for which there is a connection to ambient conditions at both portals.
The latest contribution to the development of multi-scale modelling in FDS came in the form of the PhD dissertation of Cosentino [12]. Cosentino adapted the source code of FDS to include mass and heat transfer effects into the HVAC components. This was done by implementing a new type of vent, which was called "EXCH". The results of the multi-scale model were then validated against a full CFD simulation. To this day the "EXCH" vent is however not yet available in the latest FDS release (6.6.0).
The research described above comprises -to the knowledge of the author- all of the research performed in the field of multi-scale modelling for fire. This shows that the performed research is limited and mainly focussed on traffic tunnels, with the only available experimental validation being the Dartford tunnel experiment. In this work the multi-scale approach will be adapted to an accelerator tunnel for the first time to investigate the feasibility of the concept outside traffic tunnel modelling.

2.4 Summary

This chapter introduced the multi-scale modelling concept. It was broken down into its constituent parts and these were individually discussed. Subsequently RANS, LES and network modelling were all touched upon. It was also explained how FDS handles multi-scale modelling using the HVAC components and the main limitations were emphasized. This chapter concluded by giving an overview of the already performed research with respect to multi-scale modelling for fire phenomena. The results of Colella, Vermesi and Consentino were highlighted, but it was also shown that there is still a lot of progress to be made in the field of multi-scale modelling.

Chapter 3

The LHC tunnel

Before starting any simulation it is important to understand the exact configuration of the system under consideration. This chapter will introduce the layout of the LHC accelerator and the operation of the ventilation system, two of the most important factors in understanding the development of a possible fire in a tunnel. Although the goal of this thesis is to try and present a general framework for the multi-scale modelling of accelerator tunnels, most of the parameters and geometry are derived from the LHC since this is the main accelerator currently in use at CERN.
A section of this chapter is also dedicated to the selection of a design fire. An entire thesis could be dedicated to purely identifying and defining possible fire sources and their respective heat release rates, but this is not the goal of this dissertation. This section merely presents several fire scenarios that were previously identified by the CERN fire safety engineering team in order to get a realistic feel of heat release rates, which can be encountered in an accelerator tunnel.

3.1 The Large Hadron Collider

The LHC is the main accelerator in use at the CERN site in Geneva today. It is the world's largest and most powerful particle accelerator. It was designed, aiming to discover the BEH boson and to study high energy events up to 14TeV. [3]. The LHC became operational in September 2008 and in 2012 the discovery of the BEH boson was confirmed.
The LHC accelerates two beams of particles across two 27km long rings. Before the particles are inserted into the LHC they have already passed a number of accelerators in order to reduce the energy boost that needs to be provided by the LHC, cf. figure 3.1. The protons originate from a bottle containing hydrogen, from which the electrons are stripped. The Linac2 provides the protons with their first energy boost and sends them to the PS booster. After the booster the Proton Synchrotron further boosts the energy of the protons and subsequently they are further accelerated by the Super Proton Synchrotron before being injected into the LHC [6]. To accelerate the particles to almost the speed of light superconducting magnets cooled to a temperature of -271.3 degrees Celsius are used [5]. The two

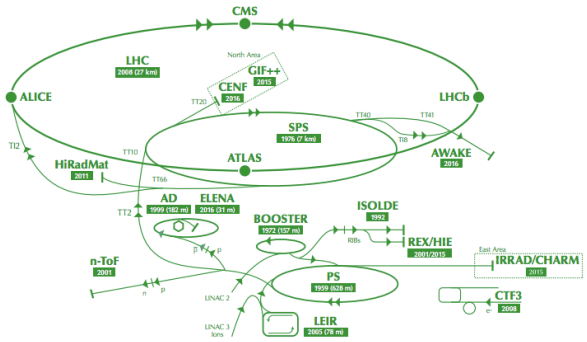

Figure 3.1: The myriad of accelerators and experiments at CERN [6]

beams intersect at four different locations where the collisions are monitored by the four main detectors: ATLAS, CMS, ALICE and LHCb. Each with their own specific goals and composition.

3.1.1 LHC tunnel layout

The LHC was built in the same 27km long circular tunnel as the former Large Electron Positron collider (LEP). A schematic of the LHC tunnel is depicted in figure 3.2. Although the schematic represents the tunnel as a circle, in reality the tunnel is a complex network of long straight sections, interlinked with curved sections and further interconnected with other accelerators for inserting the particle beams. For this thesis it suffices to think of the tunnel as a circle consisting of eight sections each three kilometre long. These sections are the "secteurs" depicted in figure 3.2. Inside the tunnel the main obstacle is the main beam ring consisting of superconducting magnets carrying the particle beam. There are also access shafts, technical caverns for ancillary electrical equipment and structures housing other equipment, which cannot be placed at the surface [4]. The tunnel itself is constructed out of pre-cast concrete with a smooth in-situ cast lining and has a diameter of roughly 3.7m. The tunnel depth varies between -45m and -170m at its deepest point.

3.1.2 The LHC ventilation system

The ventilation system in use in the LHC accelerator tunnel is a push-pull system as was discussed in section 1.4.2. Air is inserted at the even points along the tunnel and extracted at odd points. Figure 3.3 illustrates the functioning of the push-pull system. The inserted flow is split at the bottom of the insertion duct and flows to the two nearest extraction points at either side of the insertion duct. The ventilation system has several modes of operation depending on the conditions in the tunnel. In the remainder of this thesis it will be assumed that the mode of operation of the ventilation system is inserting and extracting 36000 $m^3/hour$ or

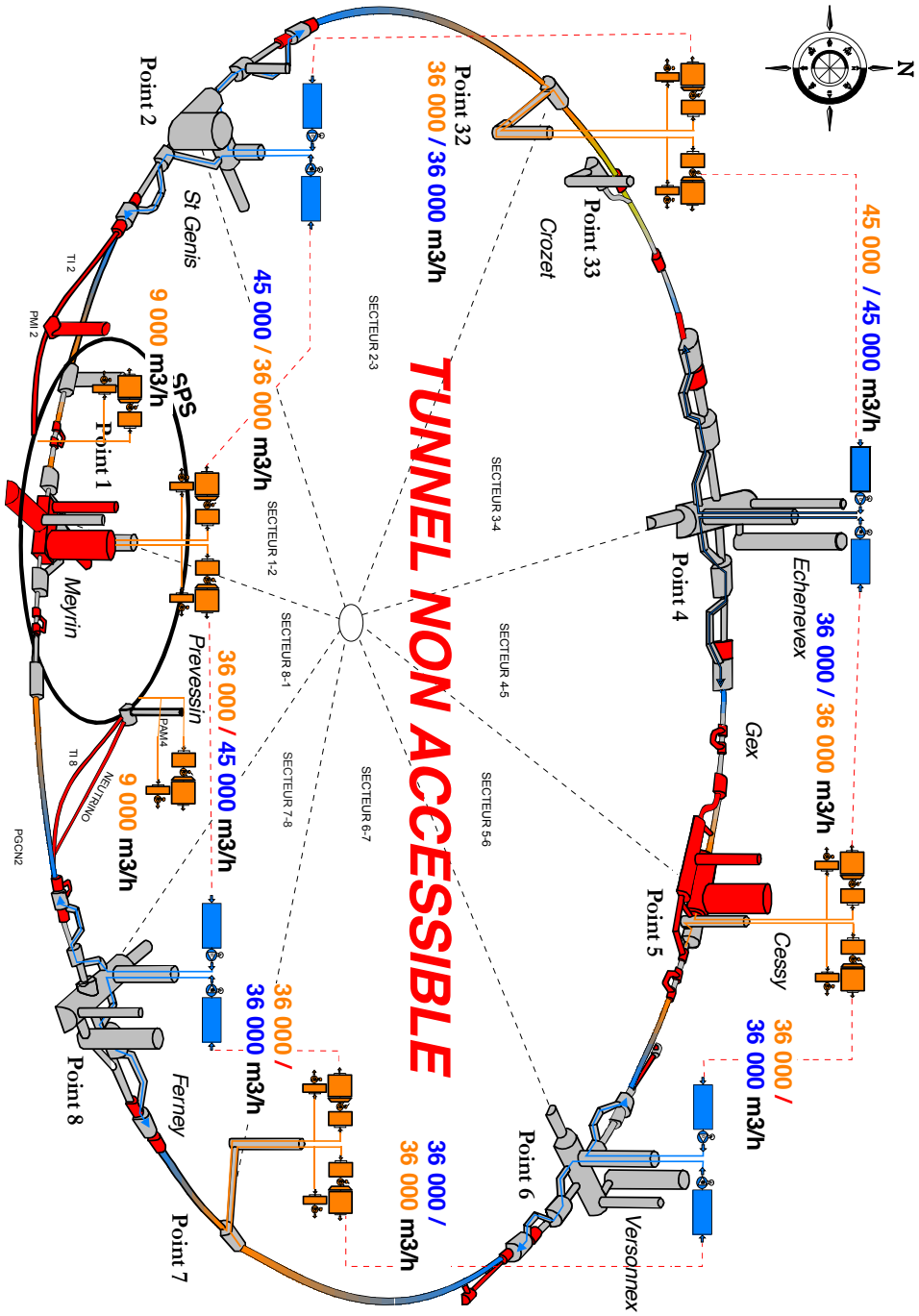

Figure 3.2: LHC layout [16]

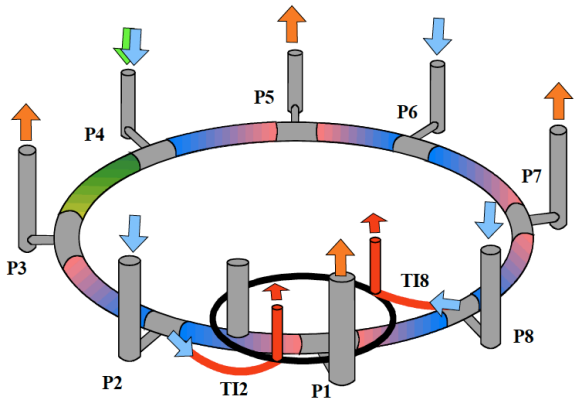

Figure 3.3: Extraction and insertion points of the LHC ventilation system [4]

10 m^3/s, through each of the insertion and extraction ducts. Although not every insertion and extraction point operates at this specific flow rate. This mode of operation is supposed to be the default operating mode of the HVAC system for the majority of the tunnel sections. The flow is provided by fans located at the surface. It is important to note that there is no compartmentalization present in the tunnel sections to impede the spread of smoke caused by a fire.
The extraction of smoke is not the only function of the HVAC system. It was mainly designed with the removal of excess heat in mind. The *LHC design report: Volume 2* [4] states the following as main functions of the HVAC system:

- Supply fresh air for people
- Provide heating and ventilation
- De-stratify the air and maintain a suitable temperature of the equipment
- Dehumidify air to prevent condensation
- Permit cold smoke extraction
- Purge the air in the tunnel before access
- Filter the exhaust air
- Attenuate sound emissions associated with the exhaust air

3.2 Design fire scenarios

Selection of a representative design fire is always a tough decision. There are so many variables involved in a fire that it is virtually impossible to exactly predict the

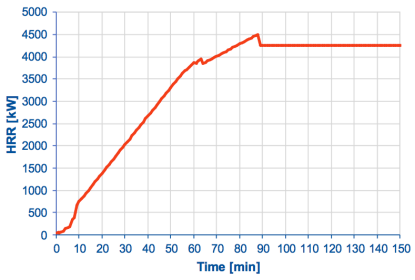

Figure 3.4: Cable tray fire [26]

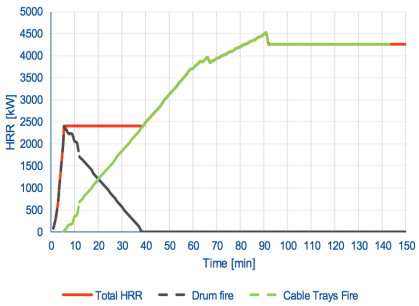

Figure 3.5: Cable drum fire [26]

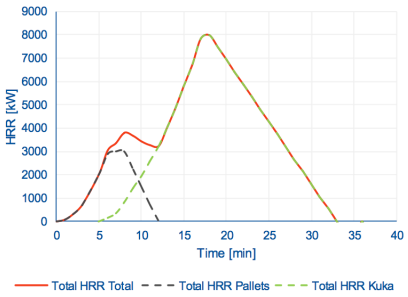

Figure 3.6: Transport vehicle fire [26]

heat release rate, yields of toxic species, yield of soot, growth rate... The solution is often to look at the most probable fire sources. In the case of the LHC tunnel risk assessments have shown that the majority of fires occurs when the accelerator itself is not operating, but when maintenance is performed. In other words when people are present in the tunnel. The scenarios that are presented in the following paragraphs stem from an analysis by the fire safety engineering team at CERN, to identify possible fire scenarios for the FCC [26].

Cable tray fire

The cable tray fire presented in figure 3.4 represents the case in which four vertically stacked cable trays catch fire. It is characterised by a slow growth rate and a steady state portion which is reached when the extinction rate matches the fire spread rate.

Cable drum fire

Figure 3.5 represents the second fire scenario suggested by the fire safety engineering team of CERN. It considers the ignition of a large (~40kg) cable drum, containing a cable spool (~50kg). The wooden drum, wrapped with cables burns quickly, reaching a peak HRR after about eight minutes. At this point it sets fire to the surrounding cable trays as in the previous scenario and after the drum and cable have been consumed by the fire it defaults to the cable tray fire as discussed before.

Transport vehicle fire

The final scenario of figure 3.6 depicts a burning transport vehicle as commonly used inside the tunnel, containing five wooden pallets. The pallets ignite first, burning quickly, after which the fire spreads and engulfs the vehicle itself as well. This scenario has the highest peak HRR and a fire growth rate that is similar to the drum fire in the first few minutes of the fire.

3.2.1 The FDS design fire

The previous paragraphs introduced several plausible fire scenarios which can occur in an accelerator tunnel. Every one of them represents a realistic HRR-curve, but when simulating a fire more practical aspects come into play as well. One such parameter is the desired simulation time. In the afore mentioned cases the fire kept growing up until 90 minutes for two of the scenarios. This is an infeasible time span to simulate due to both time and computational constraints. The transport vehicle fire on the other hand grows much faster, but does not have a steady state portion and thus does not allow the multi-scale model to be evaluated in steady state conditions.
The goal of this thesis is however not to select the most suitable fire scenario, but rather to develop a multi-scale model that in the end can serve as a basis for any design fire. In order to facilitate this, other fire characteristics are more preferable than being as realistic a fire as possible. The eventual fire used throughout this thesis therefore does not resemble any of the scenarios above.
The HRR of the fire used in this work is shown in figure 3.7. It has a fast t^2-growth during the first 50s after which it burns at a steady 1MW HRR. The fast growth is chosen to be able to see the effects of a steady state burning fire as soon as possible after the fire starts, and as such to limit the needed simulation time. The HRR of 1MW on the other hand limits the temperature of the smoke and allows for the flow to become fully developed quicker. Note that the fire only starts after 100s, to allow the ventilation system to establish a steady state flow before the fire starts. The fuel burned is taken to be polyurethane, producing a thick black smoke. Polyurethane is the same fuel as was used before by the fire safety engineering team of CERN in previous research concerning multi-scale modelling [17]. Using the same fuel and HRR of 1MW as used in previous research, facilitates the comparison of the previously obtained results. Although polyurethane is generally not present in accelerator tunnels, the thick black smoke serves as an ideal fuel for visualisation of smoke movement. It makes the visualisation of the back-layering length and the identification of the exact arrival time of the smoke at the 1D-3D interface much easier within Smokeview and thus allows for an easier validation of the results obtained from the FDS device outputs.

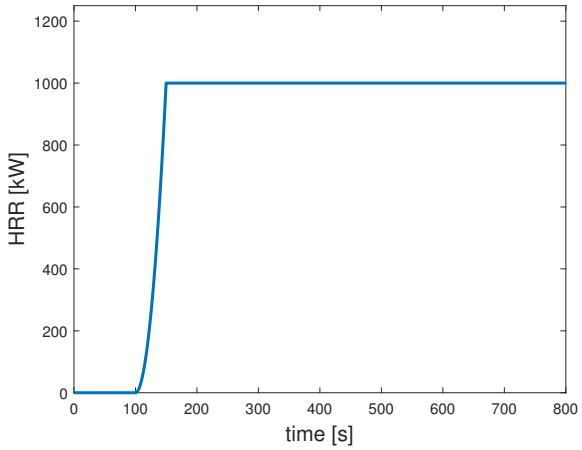

Figure 3.7: HRR of the FDS design fire used throughout this thesis

The fire is defined in FDS as follows:

```
&REAC ID='POLYURETHANE',
      FYI='NFPA Babrauskas',
      FUEL='REAC_FUEL',
      C=6.3,
      H=7.1,
      O=2.1,
      N=1.0,
      SOOT_YIELD=0.1,
      HEAT_OF_COMBUSTION=27000.0/

&SURF ID='FIRE',
      HRRPUA=1000.0,
      TAU_Q=-50/
```

3.3 Summary

Chapter three discussed the main accelerator tunnel in use at CERN today, namely the LHC tunnel. The tunnel usage, layout and functioning of the ventilation system were established and elaborated upon. The functioning of the push-pull system was explained, with insertion happening at even points, while extraction takes place at odd points around the circumference.
In a following section several fire scenarios were proposed: a stacked cable tray fire, a cable drum fire and a transport vehicle loaded with pallets fire. But eventually practical considerations led to the introduction of a custom design fire using polyurethane as a fuel.

Chapter 4

Reference case set-up

Now that the geometry of the tunnel, the type of ventilation system and the design fire are determined, the FDS simulation can be set up. The full FDS code can be referenced in appendix A. All of the results shown, which are not explicitly plotted as a function of time are shown in steady state and averaged over 15s -unless mentioned otherwise- to provide consistent results. The rationale for doing so is provided in appendix B.

4.1 System simplification

The previous chapter introduced the LHC tunnel and the push-pull ventilation system it employs. Every tunnel section is bounded by an insertion duct on one side and by an extraction duct on the other side, cf. figure 3.3. Here one such section will be subject to investigation, but in chapter 5 the system sensitivity to a bigger domain will also be analysed. Since only one section is modelled, the flow rate of $36000 m^3/s$ is halved as well, leading to a flow rate of $5 m^3/s$.
The depth of the LHC varies between -45m and -170m in reality, but here it will be assumed that the average depth of the tunnel is -100m. Both insertion and extraction ducts, thus are taken to be roughly 100m long, reaching from the surface to the tunnel itself. The horizontal portion of the domain is one section of three kilometer. This comprises both the detailed 3D domain of variable length and the 1D simplification of the remainder of the three kilometre horizontal portion. The 3D domain contains the fire source and is connected to the 1D domain at its left and right interface. The simplified system is portrayed in figure 4.1.

4.2 Fan implementation

The accelerator tunnel is modelled as being 100m beneath the ground[1]. The hydrostatic pressure drop solely due to the height difference between entry point of

[1] FDS 6.5.3 contains a bug with respect to negative z values, to circumvent this the entry points of the shafts were taken at z equal to 100m, the tunnel itself is located at z=0m.

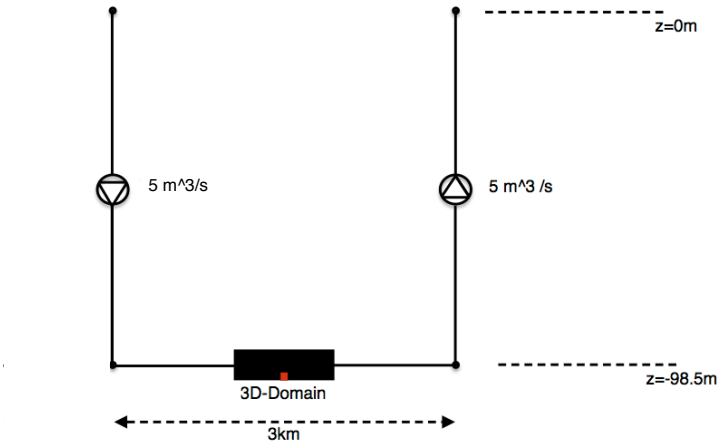

Figure 4.1: Basic part of the accelerator ring[2]

the ventilation shaft and the 3D domain is roughly 1050Pa. This means that the insertion fan has to overcome this pressure difference plus any extra dynamic losses. The extraction fan on the other hand has to overcome "minus" 1050Pa, since both fans are located at the surface.

4.2.1 The non-localised fan problem

In reality the insertion fan realises a local pressure rise across the fan. This pressure boost is then consumed by the flow on its way down the ventilation shaft to overcome the hydrostatic and dynamic pressure losses. In the HVAC module a fan is however related to a duct and the pressure difference across this duct. As a result the pressure rise realised by a fan associated with the duct is only added at the downstream node of the duct. This means that simply implementing a fan that realises a 1050Pa pressure rise causes the pressure in the horizontal portion of the system to rise with 1050Pa relative to ambient.
By splitting the vertical ducts in two parts, this problem can be circumvented. The duct is split in a 1m and a 99m portion and the fans are associated with the 1m duct. Since the pressure drop over a 1m vertical drop is negligible, the operating points of the fans can be centered around $\Delta p = 0Pa$ and the flow is set to $5m^3/s$.

FDS allows for three different ways to implement a fan associated with a duct: by defining a constant volume flow rate, a quadratic fan or a user-defined fan curve [21]. Figure 4.2 shows the different options available in FDS. The constant volumetric fan

[2] not to scale

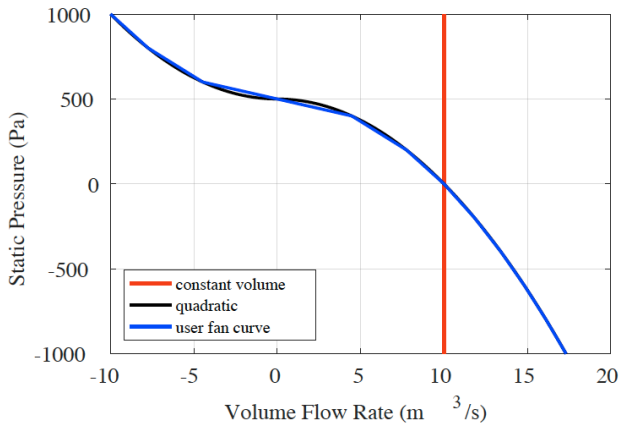

Figure 4.2: Example of a constant volumetric fan, a quadratic fan and a user defined fan [21]

is an ideal situation, but is not a robust solution as the simulations fail as soon as the flow rate deviates from the intended flow rate due to numerical instabilities. The user-defined fan is the most accurate definition when exact fan data is available, however since the fan operating point had to be shifted to $\Delta p = 0Pa$ the original fan curves cannot be used. Defining the fan as a quadratic fan with a maximum volumetric flow rate of $5m^3/s$ and a maximum pressure of $2000Pa$ allows to approximate the constant volumetric fan as close as possible while still allowing for small perturbations around the operating point of $\Delta p = 0Pa$; $\dot{V} = 5m^3/s$. It avoids the fan being represented by a purely vertical line and also allows for easy variation of the flow rate in a sensitivity analysis. The exact implementation of the extraction and insertion fan is as follows:

```
1 &HVAC TYPE_ID='FAN', ID='Fan', MAX_FLOW=5., MAX_PRESSURE=2000.,
    ↪ TAU_FAN=50.0/
```

The fan starts by following a hyperbolic tangent during the first 50 seconds, at that point it reaches steady state and the flow is allowed to get into regime for another 50 seconds before the fire is started. This prevents the fire and fan competing during the start-up phase.

4.2.2 Supply VS extraction fan

The push-pull system is such that both supply and extraction happen in a forced way. This requires the implementation of some kind of control to prevent the build-up or loss of pressure inside the tunnel. In FDS implementation of such a control system is not possible. Unlike in reality where a fan can operate on different fan curves, following a change in RPM, in FDS only one fan curve can be implemented.
Defining the system as in 4.1 leads to a hyperstatic system, as there is no flexibility for the 3D domain to deviate from the boundary conditions imposed by the two connected ducts. This leads to a highly unstable system, which fails as soon as

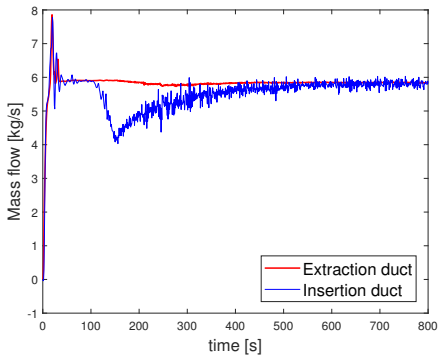

Figure 4.3: Mass flow throughout the ducts for the case with only an extraction fan

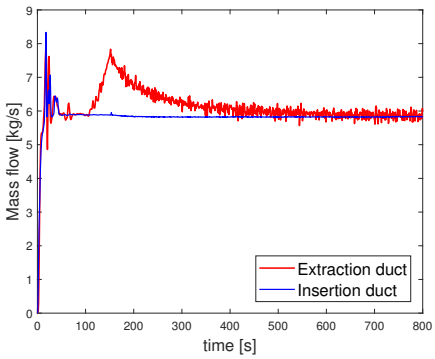

Figure 4.4: Mass flow throughout the ducts for the case with only an insertion fan

numerical instabilities occur. In order to form a robust system, the boundary conditions can only be defined on one of either interfaces of the 3D domain (left or right). Either the insertion side fan is modelled or the extraction fan.

Figure 4.3 and 4.4 compare the cases, where only an extraction or insertion fan is present. They show the mass flow through the 1D domain, during 800s of simulation. Note that it is mass flow that is shown rather than volumetric flow, as this is insensitive to changes in temperature.
As stated above the fan starts up during the first 50s and is then allowed 50 more seconds to get into regime before the fire starts. In both figures the explicitly defined side has a more stable behaviour over time, while the non-defined side exhibits a more nervous behaviour. Ignoring the initial transients during the start-up phase of the fan, one phenomenon stand out. Namely the trough and crest on the non-defined sides, which line up with the start-up phase of the fire from 100s-150s. Both of these can be explained by remembering the FDS computational flow of figure 2.4. The 3D domain is always calculated first before the HVAC-solver solves the 1D domain. In the case of the extraction fan only, the non-defined side sees an increased flow resistance as soon as the fire starts and the HVAC-solver lags behind on the amount of mass that is extracted on the other side. In the case of the insertion fan, the fire actually helps push out more mass than is being inserted on the other side.
The fact that the non-defined side lags behind is also partly attributed to the fact that the DT_HVAC parameter was set to 0.7 on the &MISC line. This forces the HVAC-solver to use DT_HVAC rather than the default FDS time step [21]. DT_HVAC=0.7 is already quite a large value, but increases the stability of the simulations, by avoiding that changes in the HVAC-solver lead to large perturbations in the 3D domain which further influence the HVAC-solver etc... This however goes at the cost of no longer being able to respond to sudden transients in the HVAC-flow [14].

The previous paragraph showed that there are two options to model the system,

either by using an insertion fan or by defining an extraction fan. In the remainder of this thesis an extraction fan will be used, unless otherwise specified. This guarantees that at the downstream node of the fire the exact boundary condition is specified, as it is here that the main interaction between smoke in the 3D domain and 1D domain will take place. The upstream node can avoid this interaction by allowing enough distance between the fire and the upstream node, since the back-layering length is limited.

4.3 Tunnel geometry

The LHC tunnel has a standard horseshoe shaped cross section. The tunnel diameter is approximately 3.7m, with a height of roughly 3m. Taking into account obstacles, such as the magnet ring, which carries the particle beams, the effective cross sectional area is about $8.4m^2$. The tunnel lining consists of smooth cast concrete. A typical absolute roughness value for cast concrete is: $\epsilon = 5 \times 10^{-4}m$ [24] and will be used as roughness for the horizontal ducts. The vertical ventilation shafts are assumed to be constructed out of metal, the absolute roughness is taken to be $\epsilon = 5 \times 10^{-5}m$ [24] one order of magnitude smaller than the horizontal ducts. Specifying a roughness for the ducts is important as not doing so would lead to a zero loss coefficient, leading to unstable simulations.

The LES-implementation used in FDS uses a logarithmic law of the wall model. The roughness of the 3D domain is specified by defining a "sand grain" roughness [21]. By doing so the default logarithmic model is interchanged for the logarithmic law of the wall model defined by Pope [20]. Unlike not specifying a roughness for a duct, not specifying a roughness for the 3D domain does not lead to stability problems for the simulation as by default a smooth wall is assumed.
Since the exact properties of the concrete lining the tunnel are not known it is opted to use the default inert boundary condition for the tunnel walls. The correctness of this default boundary condition will later be tested in chapter 5.

4.3.1 Tunnel shape

FDS only allows rectilinear volumes to be used to define the domain and obstacles, making it impossible to exactly model a round shape, such as a tunnel. The horseshoe shape can however be mimicked by creating a stair-stepped tunnel as was performed in figure 4.5. The major flaw in this design is the extra turbulence that is created at every edge. From a fluid dynamic point of view the fluid flow will be completely different from a tunnel with a smooth wall. Another argument against a stair-stepped tunnel comes from the default FFT pressure solver. The FFT solver tries to force the normal component of the velocity to zero on every obstacle inside the 3D domain [21]. Since the stair-stepped tunnel is completely built up out of obstacles this results in a very slow and unstable simulation. A solution to this last problem might be provided by the optional GLMAT solver, introduced in FDS 6.6.0. But this has not

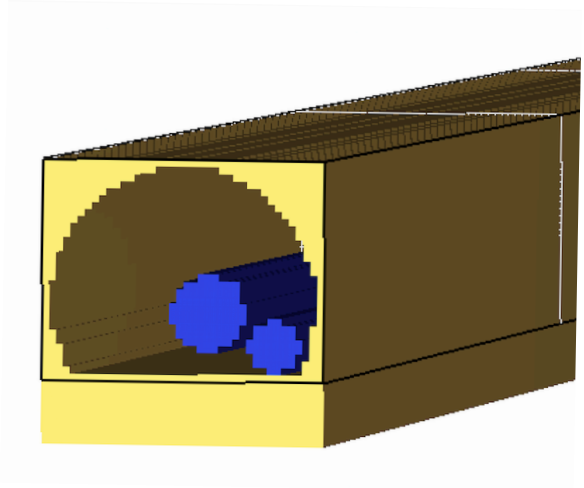

Figure 4.5: Stair-stepped model of the LHC tunnel

been tested in this thesis.

Since the stair-stepped model alters the fluid flow properties, the tunnel will instead be modelled by using a simple rectangular cross section. The height of the tunnel is maintained at three meter and the original effective cross section of $8.4m^2$ is also maintained. This leads to a rectangular tunnel: $3m$ high and $2.8m$ wide with a hydraulic diameter of $D_h = \frac{4A}{P} = 2.9m$. The 1D ducts are constructed using the same parameters.

4.3.2 Tunnel length

The considered system has a horizontal portion of 3km long. Part of this is modelled in 3D and the remainder is modelled using HVAC ducts. The question now arises, how long the 3D domain should be in order to get correct results. The notion of correct results itself should however be clarified. One should always remember that the results of a simulation should be met with a healthy dose of scepticism, since they are the result of a number of assumptions that do not capture reality in its entirety. Here the matter is complicated even further by the fact that there is no experimental basis to validate the results. Section 2.1.3 already highlighted that the theoretical basis for coupling 1D and 3D CFD is based on the assumption that the 3D flow has become essentially 1D at the position of the interface between the 1D and 3D domain. This will also form the notion of correctness in this report. More specifically both temperature and velocity profiles of the flow will be analysed over the height of the tunnel. As soon as these no longer show strong gradients over the height the flow can be assumed to be one-dimensional and the solution to be correct. The 3D domain can be thought of as consisting out of two pieces, a section upstream of the fire and one downstream.

Figure 4.6: Back-layering of the smoke as seen in smokeview in steady state

Upstream length

If the ventilation velocity in a tunnel is not high enough, part of the smoke will spread upstream of the fire. A phenomenon know as back-layering. The hot smoke sticks to the ceiling of the tunnel and cold fresh air flows towards the fire source underneath. Cold air is moving in one direction and hot smoke in the other, making it impossible to obtain a 1D velocity profile within the the back-layering region. The back-layering is thus an important parameter in determining how long the upstream length of the 3D domain should be. Li [18] proposed the following expression, to correlate back-layering length, HRR and longitudinal ventilation velocity:

$$L_b^* = \frac{L_b}{H} = \begin{cases} 18.5 \ln\left(0.81 Q^{*1/3}/u^*\right) & Q^* \leq 0.15 \\ 18.5 \ln\left(0.43/u^*\right) & Q^* \geq 0.15 \end{cases} \tag{4.1}$$

With Q^* and u^* the non-dimensional HRR and velocity given by:

$$Q^* = \frac{\dot{Q}}{\rho_0 c_p T_0 g^{1/2} H^{5/2}} \quad \text{and} \quad u^* = \frac{u}{\sqrt{gH}} \tag{4.2}$$

Entering $\dot{Q} = 1000kW$, $H = 3m$, $u = \frac{5m^3/s}{8.4m^2}$ and all other properties evaluated at $T_0 = 293K$ this leads to:

$$L_b \approx 64m$$

Figure 4.6 allows to verify this calculation. It shows a back-layering of 74m of the smoke for a 640m long 3D domain, with a length of 140m upstream of the fire, during steady state conditions. The ticks are spaced 10m apart and the fire is indicated by the red dot, originating at 4m from the first tick. In smokeview it can further be seen that the back-layering length steadily increases during the start-up phase of the fire and attains a stable value of 74m in steady state, which is in good agreement with the value calculated earlier. This suggests that the absolute minimum length of the upstream domain must be at least equal to 74m, to obtain a 1D profile. The question however arises if this is a sufficient and/or a necessary condition for the upstream domain length.

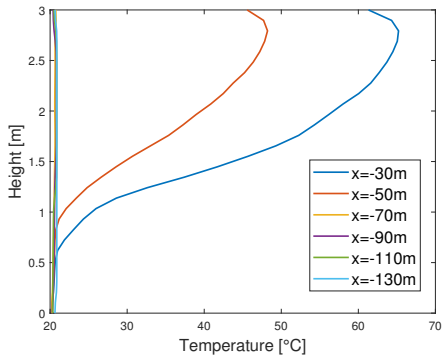

Figure 4.7: Temperature profiles at different points along the 3D domain

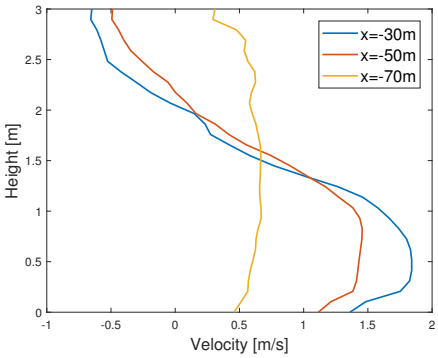

Figure 4.8: Velocity profiles at different points along the 3D domain within the back-layering region

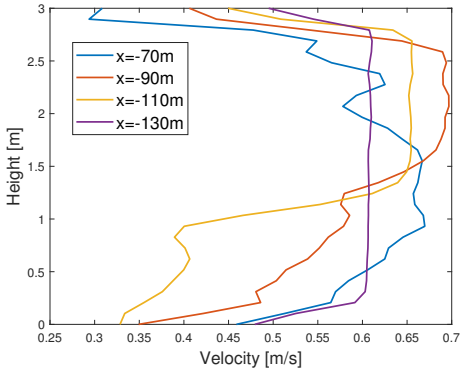

Figure 4.9: Velocity profiles at different points along the 3D domain upstream of the back-layering region

Figure 4.7 illustrates that with respect to temperature it serves as a sufficient condition. The fire source is located at x=4m[3] and at x=-70m the temperature profile shows no variation over the height of the tunnel, satisfying the 1D condition. The velocity profiles over the tunnel height within the back-layering region and upstream of the back-layering region are shown in figures 4.8 and 4.9. These display the component of the velocity vector along the length of the tunnel, which is positive in the downstream direction and negative in the upstream direction. Within the back-layering region it is clear that the flow is bi-directional, with hot smoke moving upstream and cold fresh air flowing towards the fire at the bottom of the tunnel. This behaviour is observed up until the back-layering length L_b at x=-70m where the ventilation velocity reaches its default value of $\frac{5m^3/s}{8.4m^2} \approx 0.6m/s$ across the cross section of the tunnel. At first sight it might seem that the sufficient condition also holds with respect to the velocity component. However when looking at the velocity

[3]The positioning of the fire source at x=4m and not at x=0m allows it to be placed in the middle of a mesh, as will be clarified later.

profiles upstream of the back-layering region, cf. figure 4.9 it becomes clear that the flow development is quite complex after the insertion in the tunnel at x=-140m, even when abstraction is made of the formation of boundary layers at top and bottom of the tunnel. At x=-130m right after the insertion the flow can still be considered 1D, but moving in the positive x-direction the flow becomes more complex and loses its 1D profile. To allow for this flow development, it is opted here to use a total 3D domain length upstream of the fire of 144m. This is a conservative approach, but since no experimental validation is possible at this time, this case will serve as a reference for simulations to come and it is preferred to err on the side of caution. In chapter 5 it will be checked if this approach is overly conservative.

Downstream length

Determination of the needed length of the 3D domain downstream of the fire is the second step in determining the total domain length of the 3D domain. It was suggested by Colella in [9] that a downstream distance of $L_d = 13 \times D_h$ is the minimum distance that should be respected between the fire and the downstream interface. In casu this means a length $L_d \approx 40m$. Looking at figure 4.10 it becomes clear that the temperature profile does not resemble a 1D profile until about 250m downstream of the fire, a lot more than the first suggested 40m. A possible cause for the difference in findings could be the difference in tunnel cross section between the research of Colella and the LHC tunnel. The road tunnels which were the subject of Collela's research were much bigger than the LHC tunnel having relatively a much larger heat sink than the LHC tunnel. Furthermore the available height over which the rising smoke plume can entrain air is severely limited in the LHC tunnel as well, due to the ceiling being only 3m high. Another factor playing a role is the fact that ventilation speed in Collela's case was much higher than 0.6m/s.
Figure 4.11 provides a close-up of the temperature profiles that resemble a one 1D-profile. The deviation from the mean temperature for the minimum and maximum temperature along the profile is given in table 4.1, as is the relative total deviation from average[4] encountered along the profile.

	mean temperature	**max deviation**	**min deviation**	**rel. total deviation from average**
$\boldsymbol{x = 250m}$	24.2°C	4.7%	-10%	14.7%
$\boldsymbol{x = 350m}$	21.5°C	2.5%	-4.3%	6.8%
$\boldsymbol{x = 450m}$	20.6°C	1.5%	-2.3%	3.8%
$\boldsymbol{x = 490m}$	20.4°C	1.1%	-1.6%	2.7%

Table 4.1: Relative difference in temperature at different positions downstream of the fire

[4]The metrics used are defined in appendix B

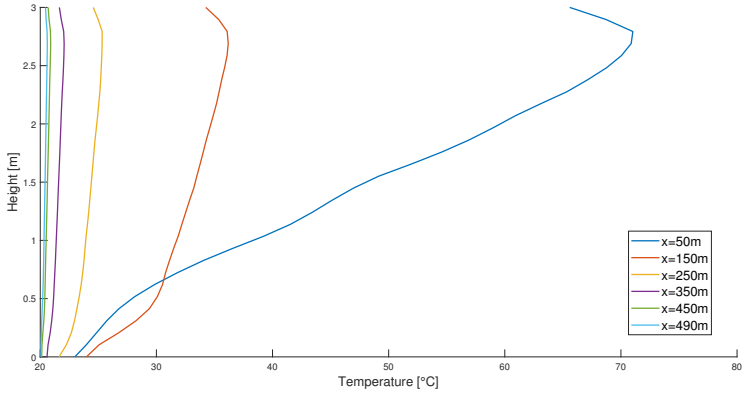

Figure 4.10: Temperature profiles at steady state for different x-values downstream of the fire

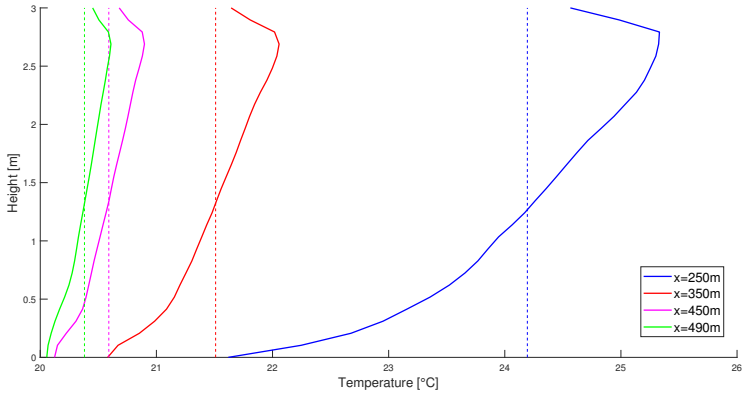

Figure 4.11: Close-up of steady state temperature profiles at different x-values downstream of the fire. Average temperatures are indicated by dashed lines.

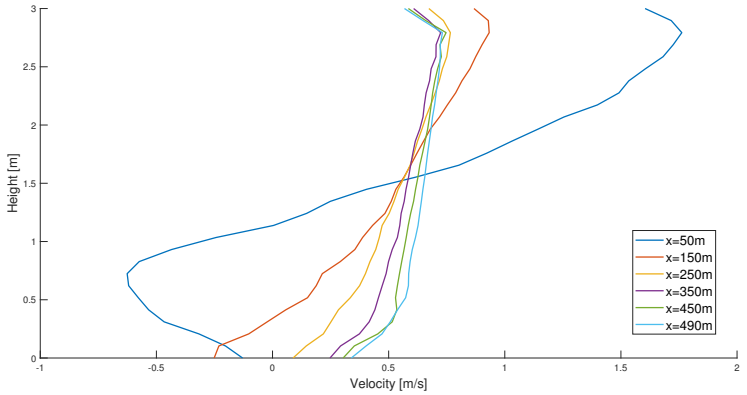

Figure 4.12: Velocity profiles at steady state for different x-values downstream of the fire

Whereas the relative total deviation from average at 250m is still 14.7%, this is more than halved a 100m further down the tunnel down to 6.8%. From a temperature profile perspective a distance of 350m downstream of the fire is arguably enough to justify the assumption of a one-dimensional profile as the total relative deviation from average is well under 10%.

The same analysis is repeated for the velocity profile along the tunnel. The results are shown in figure 4.12. At first sight it seems that once again for a distance of 350m downstream of the fire the velocity profile becomes one-dimensional. It is however evident when looking at the results in table 4.2 that the relative differences are much larger than was the case for the temperature profiles. These results should however be met with caution, since in physical reality the no-slip condition would also lead to large relative velocity differences close to the walls. From figure 4.9 it is moreover evident that even directly after the insertion interface (where the velocity is constant over the cross section) at x=-130m there is a large relative velocity difference close to the walls. Another argument suggesting that 350m suffices as downstream domain length is given by the mean velocity which almost attains the boundary condition value of 0.6 m/s at 350m.

	mean velocity	**max deviation**	**min deviation**	**rel. total deviation from average**
$\boldsymbol{x = 250m}$	0.52 m/s	46.6%	-83%	129.6%
$\boldsymbol{x = 350m}$	0.56 m/s	29.6%	-55.7%	84.6%
$\boldsymbol{x = 450m}$	0.6 m/s	24.5%	-49.3%	73.8%
$\boldsymbol{x = 490m}$	0.62 m/s	17.9%	-45.3%	63.2%

Table 4.2: Relative difference in velocities at different positions downstream of the fire

A final check of the downstream domain length can be performed by calculating the local Froude number as was explained in section 2.1.2. When the Froude number attains a value greater than 3.2 the flow can be assumed to be fully developed [15]. Different definitions of the Froude number are used throughout the literature. Newman defines it as follows:

$$Fr_{nm} = \frac{u_{avg}}{\left(\frac{\Delta T_{cf}}{T_{avg}} gh\right)^{1/2}} \tag{4.3}$$

With $u_{avg} = u\frac{T_{avg}}{T_0}$, where T_{avg} is the average temperature over the cross section and with ΔT_{cf} the difference between the gas temperature at a height $z = 0.88H$ and a height $z = 0.12H$.
Ingason uses a slightly different definition in the *Handbook of tunnel fire safety* [2]:

$$Fr_{ing} = \frac{u_{avg}^2}{1.5\frac{\Delta T_{avg}}{T_{avg}} gh} \tag{4.4}$$

With $\Delta T_{avg} = T_{avg} - T_0$ the average gas temperature rise above ambient over the entire cross section of the tunnel [2].

	$50m$	$150m$	$250m$	$350m$	$450m$	$490m$
Fr_{ing}	0.09	0.14	0.45	1.37	4.15	7.11
Fr_{nm}	0.09	0.33	1.18	2.89	5.99	7.74

Table 4.3: Froude numbers in steady state for increasing distances downstream of the fire

The results of such a calculation are shown in table 4.3. It shows that the Froude number[5] as defined by Ingason is the most conservative value and that the flow becomes fully developed somewhere in the region between 350m and 450m downstream of the fire, which is in good agreement with the results obtained earlier.

The results obtained in this section suggest that a downstream domain length of more than 350m should suffice to ensure a 1D profile at the downstream interface. Once again the reader is reminded that since no experimental validation is possible at this time, it is important to provide an as accurate as possible reference case. For this reason it is decided for now to take a domain length of 500m downstream of the fire to ensure a fully developed flow. Later, in chapter 5 it will be investigated how a change in downstream domain length influences the results and if this assumption is overly conservative.
The previous sections established that an upstream domain length of 140m and a downstream length of 500m should lead to correct[6] simulation results. The total 3D domain length for the reference case is thus 640m. Since the total section length is 3km, the upstream duct is taken to be $\frac{3000m}{2} - 140m = 1360m$ and the downstream duct is $\frac{3000m}{2} - 500 = 1000m$.

4.4 Mesh selection

The previous sections established the entire lay-out of the reference case. The main points are repeated here for clarity and displayed in figure 4.13:

- The 3D tunnel has a rectangular cross section, 3m high and has inert walls.
- The total simulation time is set to 800s, steady state mass flow is reached at 550s, leaving 250s open to steady state operation.

[5]The Matlab code used for calculation of the Froude numbers is given in appendix A.
[6]The notion of correctness was defined earlier, cf. section 4.3.2

- A 1MW fire placed at roughly x=0m is used, with a t^2-growth from 100s-150s.
- Only the extraction fan is defined, with a volumetric flow rate of $5m^3/s$.
- The vertical ducts are 100m long.
- The upstream domain is taken to be 140m long, the upstream duct is 1360m long.
- The downstream domain is 500m long, the downstream duct 1000m.

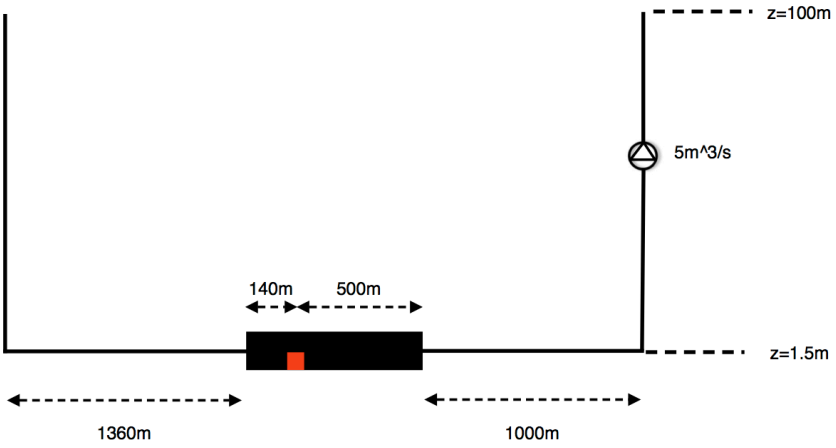

Figure 4.13: The case that serves as reference case throughout this thesis

The only question that remains, is what cell size to use. By performing a grid sensitivity study the following section will try and answer that question.

4.4.1 Grid sensitivity study

To speed up the simulations the 3D domain is split into 20 meshes, each 32m long. Every mesh is assigned its own MPI process and is supported by 8 OpenMP threads, allowing to take full advantage of the computational power provided by the HPC-cluster at CERN. By breaking up the domain in multiple meshes every process is considered as a different flow field and thus has its own boundary conditions [21]. This is the main downside of splitting up the 3D domain in multiple meshes: as the number of mesh to mesh communications increases so do the sources of error [21]. It is also the reason behind the fire placement at x=4m. This ensures the fire is located in the middle of a mesh, to reduce the error at the mesh boundaries as much as possible and to increase the stability of the simulation.

The LES approach to solving the Navier-Stokes equations followed by FDS 6.5.3, implies that increasing the mesh resolution will bring the simulation closer and closer to DNS. However refining the mesh also means increasing the computational time needed to come up with a solution. Halving the grid size in FDS theoretically results

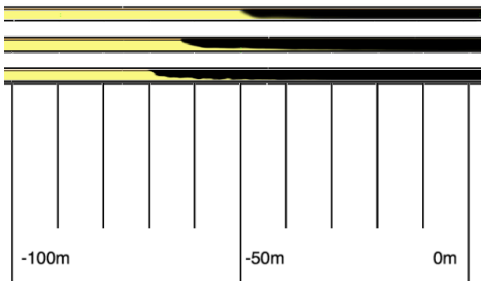

Figure 4.14: Back-layering distances for the coarse, medium and fine mesh in steady state

in a computational time increase of 16 (doubling the number of cells in 3 dimensions and halving of the time step). To get an initial idea of the grid size needed - for a simulation where the buoyant plume is the main parameter of interest - the ratio of $D^*/\delta x$ can be used. D^* is a characteristic length scale of the fire and is given by:

$$D^* = \left(\frac{\dot{Q}}{\rho_0 c_p T_0 \sqrt{g}} \right)^{2/5} \tag{4.5}$$

Inserting a value of 1000kW results in a $D^* = 0.96$. As a rule of thumb it is often suggested that the value D^* should range from 4 to 16. This implies that the maximum dimension of a grid cell should be no more than 24cm in the bounding case of D^* equalling four. It should however be remembered that this is not a be all and end all magical interval that guarantees a correct representation of reality, but at least it gives a good starting value. Three different cell sizes are evaluated:

$$\delta x \times \delta y \times \delta z = \begin{cases} 0.5m \times 0.4m \times 0.5m \\ 0.2m \times 0.2m \times 0.2m \\ 0.2m \times 0.1m \times 0.1m \end{cases}$$

A coarse, medium and fine mesh respectively. The coarse and fine mesh deviate from an aspect ratio of one, for two different reasons. In the y-direction, the mesh is 2.8m wide. Thus in case of the coarse mesh a cell size of 0.4m in the y-direction leads to 7 cells in that direction, guaranteeing that the correct tunnel dimensions are maintained. In the case of the fine mesh, reducing the x-component to 0.1m as well led to computational problems, causing the simulation to become unstable for unclear reasons.

Analysing both the upstream and downstream portion of the domain, it stands out that as the mesh size is refined, the back-layering length becomes larger, as shown in figure 4.14. This can be explained by looking at the temperature profile upstream of the fire, for example in steady state at x=-30m, figure 4.15 shows that the temperature in the smoke layer is higher as the mesh is refined. The smoke has

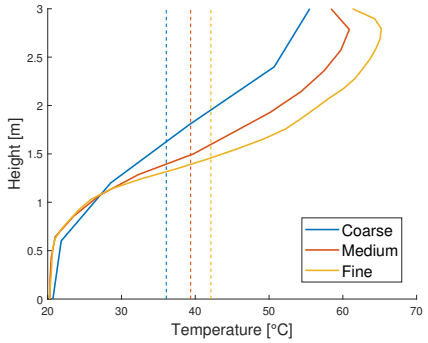

Figure 4.15: Temperature profiles for fine, medium and coarse meshes at x=-30m in steady state. The dashed lines indicate the average values.

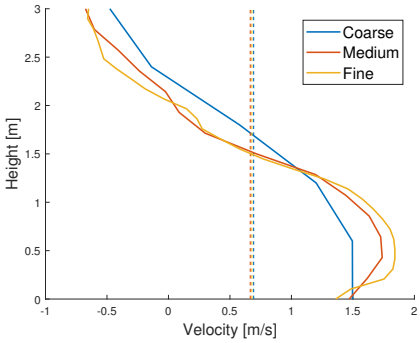

Figure 4.16: Velocity profiles for fine, medium and coarse meshes at x=-30m in steady state. The dashed lines indicate the average values.

	$\Delta T_{avg,coarse}$	$\Delta T_{avg,medium}$
$x = -30m, t = 800s$	13.6%	5.3 %
$x = 20m, t = 150s$	18 %	3%
$x = 200m, t = 800s$	1.9 %	0.6%

Table 4.4: Relative mean deviation from the fine mesh temperature profile for the coarse and medium mesh sizes

more buoyancy and flows further upstream before succumbing to gravity. Close to the fire, the velocity profiles are similar, but further upstream they are different due to the difference in back-layering length.
Downstream of the fire it can be seen that convergence has set in when comparing the results of the medium and fine mesh, both during start-up of the fire and during steady state. Results are shown in figures 4.17 to 4.20, close to the fire at x=20m after 150s and further from the fire at x=200m during steady state. While there is still some difference between the coarse and medium meshes, the medium and fine meshes show similar results.
The visual results are verified by the results summarised in table 4.4, showing the average deviation of the coarse and medium mesh temperatures over the height of the tunnel, in comparison to the fine mesh. The relative deviation for the velocity profiles is not shown numerically, since the values around zero, badly skew the results and it is easier to verify the results visually.

Computationally, the difference in cell sizes makes a big difference. Whereas the coarse mesh only takes 5 min 20s to complete, the medium mesh finishes in 2h 6min 45s and the fine mesh in 18h 40min 10s. The computational parameters are summarised in table 4.5. In appendix C the computational parameters of every simulation mentioned in this thesis are listed. Due to the fact that the simulations

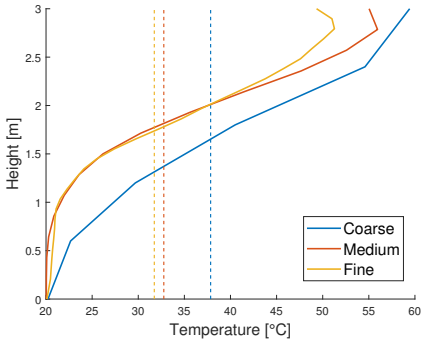

Figure 4.17: Temperature profiles for fine, medium and coarse meshes at x=20m after 150s, with the average values given by the dashed lines.

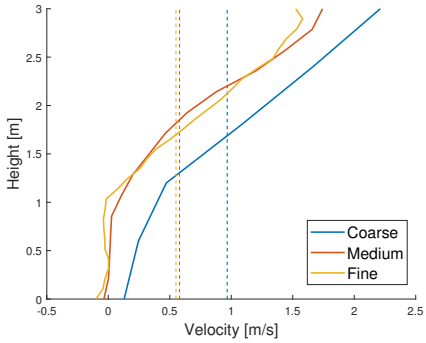

Figure 4.18: Velocity profiles for fine, medium and coarse meshes at x=20m after 150s, with the average values given by the dashed lines.

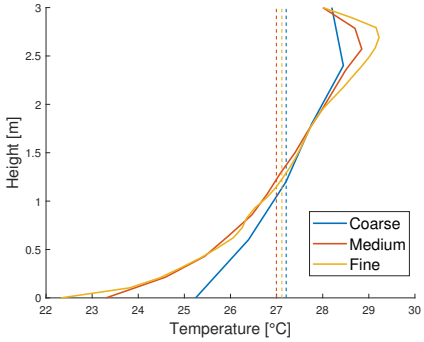

Figure 4.19: Temperature profiles for fine, medium and coarse meshes at x=200m in steady state, with the average values given by the dashed lines.

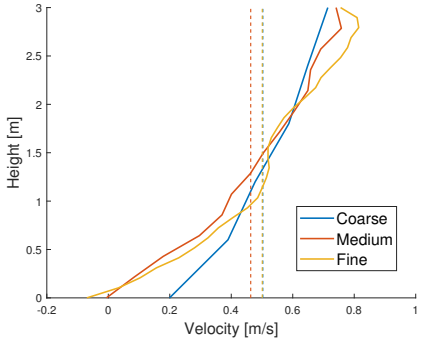

Figure 4.20: Velocity profiles for fine, medium and coarse meshes at x=200m in steady state, with the average values given by the dashed lines.

can be run without a time limit on the CERN HPC-cluster, the fine mesh is used throughout the remainder of this thesis, as to obtain as accurate results as practically possible. It should be noted that previously mentioned results have also been obtained using the fine mesh.

simulation	**# cells per mesh**	**# meshes**	**total # cells**	**cores per mesh**	**core -hours**	**Nodes**
coarse	$64 \times 7 \times 6$	20	53 760	8	14.24	be-short
medium	$160 \times 14 \times 15$	20	672 000	8	338	be-short
fine	$160 \times 28 \times 30$	20	2 688 000	8	2987.1	be-short

Table 4.5: Computational characteristics for different cell sizes

4.5 Summary

The reference case introduced in this chapter, will serve as the benchmark throughout this thesis. The tunnel geometry used is not an exact copy of reality, but by opting for a rectangular rather than a round tunnel the portrayal of the flow is more accurate from a fluid dynamic point of view. It was also shown that the lack of control in FDS made an exact representation of the push-pull system impossible, since this would lead to a hyperstatic system. In the end an extraction fan was chosen rather than an insertion fan, as this guarantees the correct boundary condition at the downstream interface. The final step in building the geometry of the reference case was deciding on the needed tunnel length. Both the upstream and downstream portion were looked at and inspected for their 1D similarity. The result was a conservative 3D domain length of 640m. The chapter concluded with a sensitivity study of the mesh to be used, leading to an eventual cell size of $0.2m \times 0.1m \times 0.1m$.

Chapter 5

Sensitivity studies

The reference case introduced in the previous chapter, represents only a section of the LHC tunnel and features a number of simplifying assumptions. In this chapter these assumptions will be put to the test by changing both 1D and 3D boundary conditions. Doing so opens the door for building an increasingly complex, but also more realistic system that consumes only as much computational time as necessary. The simulations in this chapter were all run using a mesh of $\delta x \times \delta y \times \delta z = 0.2m \times 0.1m \times 0.1m$.

5.1 1D sensitivity

Section 4.2 already compared a system with only an insertion fan to the system with only an extraction fan, which was later taken to the reference case. Both of these cases considered only one section of LHC tunnel. By expanding this to two sections, the sensitivity of the results in the 3D domain can be checked to variations in the 1D domain. Figures 5.1 and 5.2 show how the extraction and insertion fans are implemented in a system comprising two sections.

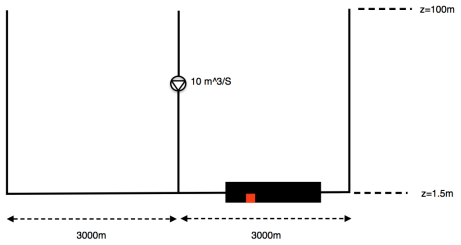

Figure 5.1: Schematic representation of the extended system with only an insertion fan

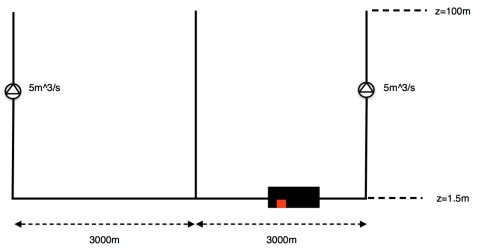

Figure 5.2: Schematic representation of the extended system with only extraction fans

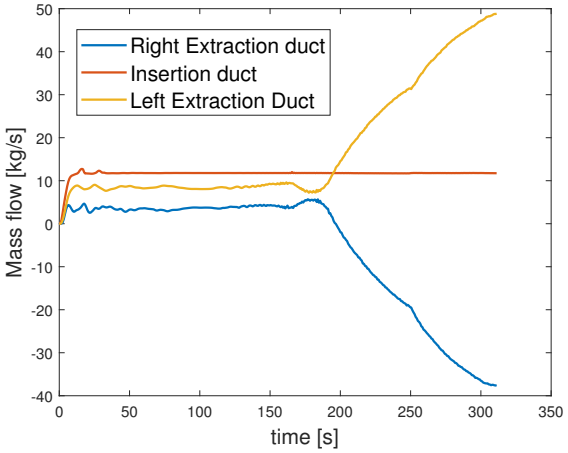

Figure 5.3: Mass flow for the extended system with only an insertion fan

5.1.1 Insertion fan

The system shown in figure 5.1 comprises only one fan, but since it now consists of two sections the flow rate should be doubled. The insertion fan now inserts $10m^3/s$ rather than $5m^3/s$. Since both the section left and right of the insertion duct are equal in length, the insertion flow was expected to split into two separate flows of $5m^3/s$ at the bottom of the insertion duct.
Figure 5.3 shows however that the system behaves differently. The flow through the section without the 3D domain is higher and eventually the flows diverge and the simulation fails. Adding an extra flow resistance to the left side of the domain did not fix this problem. A possible explanation for this behaviour is that the 3D domain is solved previous to the 1D domain. This causes the solver to always "see" a larger resistance in the part with the 3D domain, eventually leading to the divergent behaviour of figure 5.3.

5.1.2 Extraction fan

Alternatively the system can be expanded to two sections as shown by figure 5.2, with one extraction fan in each extraction duct and no boundary condition on the insertion duct. This time the system does behave as expected, with a stable flow in both sections of the system. The mass flows further suggest that the left and right sections behave independently. When compared to the mass flow of the reference case, cf. figure 4.3, the insertion mass flow is offset by the value attained in the left section but otherwise exhibits exactly the same behaviour. This is confirmed by figure 5.5 and 5.6 which compare temperature and velocity profiles for the reference case and the extended system with extraction fan.

Extending the 1D domain to include multiple sections, thus does not lead to different

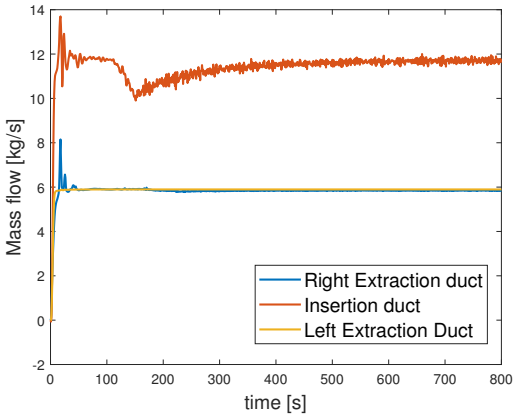

Figure 5.4: Mass flow for the extended system with only extraction fans

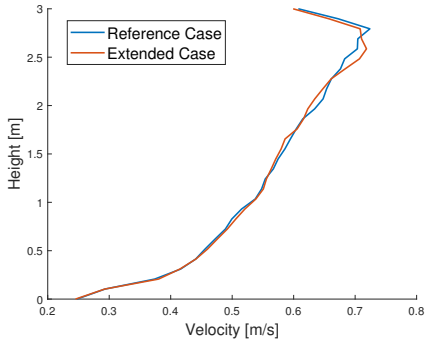

Figure 5.5: Velocity profile at 350m downstream in steady state conditions

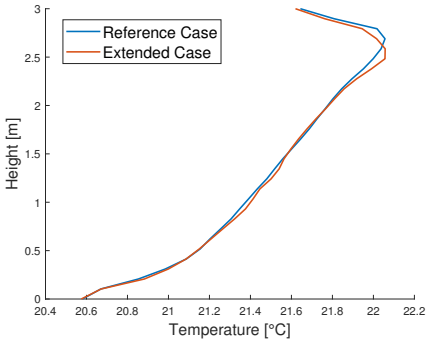

Figure 5.6: Temperature profile at 350m downstream in steady state conditions

results. In the case of the insertion fan, it even caused the simulation to crash. This suggests that extending the 1D domain without including extra 3D domains does not increase the accuracy of the results.

5.2 Sensitivity to flow rate

The length of the 3D domain is one of the most important parameters in the multi-scale model. In chapter four it was shown that the Froude number served as a good indicator of the needed downstream domain length in the reference case. By changing the flow rate this section analyses how the ventilation speed affects the development of the flow and thus also the length of the downstream 3D domain. The volumetric flow rate is increased from $5m^3/s$ in the reference case up till $20m^3/s$ in steps of

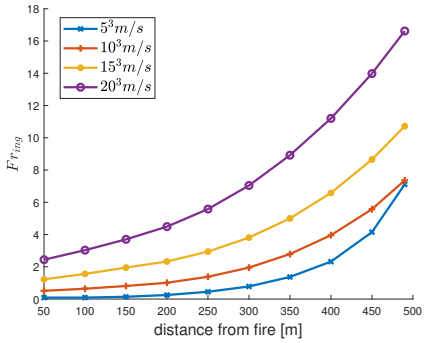

Figure 5.7: Visual representation of the development of Fr_{ing} with increasing distance from the fire

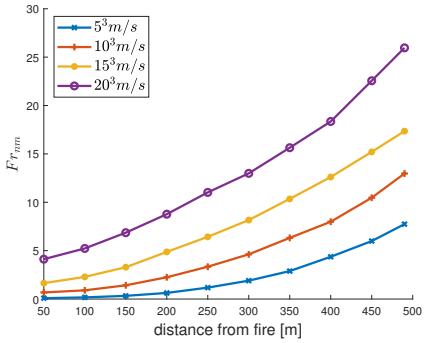

Figure 5.8: Visual representation of the development of Fr_{nm} with increasing distance from the fire

	$5m^3/s$	$10m^3/s$	$15m^3/s$	$20m^3/s$	$5m^3/s$	$10m^3/s$	$15m^3/s$	$20m^3/s$
x=50	0.09	0.51	1.22	2.44	0.09	0.68	1.64	4.12
x=100	0.09	0.64	1.56	3.03	0.17	0.9	2.29	5.23
x=150	0.14	0.81	1.95	3.7	0.33	1.42	3.29	6.86
x=200	0.25	1.01	2.33	4.49	0.63	2.25	4.87	8.77
x=250	0.45	1.38	2.94	5.58	1.18	3.34	6.43	11.02
x=300	0.78	1.95	3.81	7.04	1.9	4.62	8.16	12.99
x=350	1.37	2.79	5	8.92	2.89	6.32	10.35	15.64
x=400	2.32	3.96	6.58	11.2	4.37	7.99	12.61	18.35
x=450	4.15	5.57	8.65	13.98	5.99	10.47	15.21	22.56
x=490	7.11	7.36	10.72	16.62	7.74	12.97	17.35	25.96

Table 5.1: Froude number as defined by Ingason on the left, as by Newman on the right

five, this translates in flow speeds of $0.6m/s$, $1.2m/s$[1], $1.8m/s$ and $2.4m/s$. Table 5.1 displays the Froude numbers for different ventilation velocities, all obtained in steady state in a 3D domain with length 640m, equal to the reference case. The first Froude number greater than 3.2 is indicated in red. The left-hand side provides the Froude numbers as defined by Ingason, the right-hand side as defined by Newman. A graphical representation is also given in figures 5.7 and 5.8 for Fr_{ing} and Fr_{nm} respectively. The Froude number as defined by Ingason proves once again to be the more conservative value. The results show clearly that with increasing ventilation speed the flow becomes fully-developed closer to the fire.

The results of table 5.1 can be verified by analysing the temperature and velocity profiles at both the distance specified by $Fr_{ing} = 3.2$ and $Fr_{nm} = 3.2$, the profiles

[1] Actually a flow rate of $10.4m^3/s$ rather tan $10m^3/s$ is used, as values between $10m^3/s$ and $10.3m^3/s$ led the simulation to crash for unclear reasons.

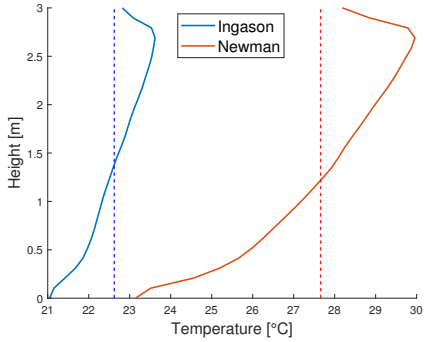

Figure 5.9: Temperature profiles: $10m^3/s$. Dashed lines indicating average values.

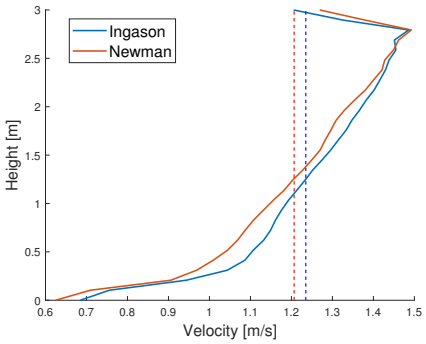

Figure 5.10: Velocity profiles: $10m^3/s$. Dashed lines indicating average values.

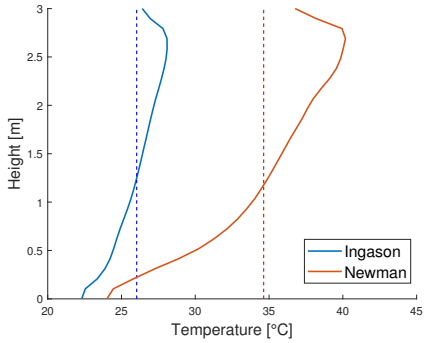

Figure 5.11: Temperature profiles: $15m^3/s$. Dashed lines indicating average values.

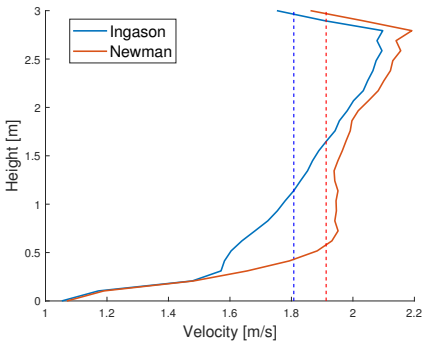

Figure 5.12: Velocity profiles: $15m^3/s$. Dashed lines indicating average values.

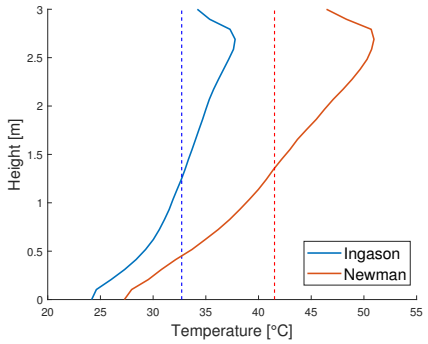

Figure 5.13: Temperature profiles: $20m^3/s$. Dashed lines indicating average values.

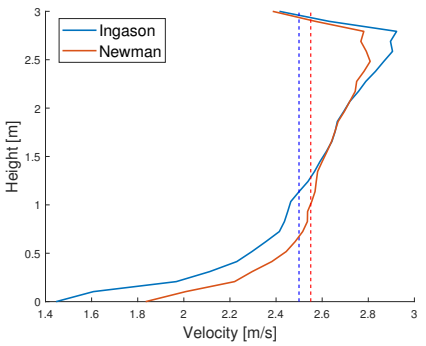

Figure 5.14: Velocity profiles: $20m^3/s$. Dashed lines indicating average values.

	$T_{avg,ing}$	$\Delta T_{max,ing}$	$T_{avg,nm}$	$\Delta T_{max,nm}$
$5m^3/s$	20.6°C	3.8%	21°C	4.8%
$10m^3/s$	22.6°C	11.3%	27.7°C	25%
$15m^3/s$	26°C	22%	32.6°C	47%
$20m^3/s$	32.7°C	42%	41.5°C	57%

Table 5.2: Relative differences in max-min temperature for positions given by Ingason and Newman

are given in figures 5.9 till 5.14, the figures for a flow rate of $5m^3/s$ are not repeated here, since they were extensively analysed in chapter 4. From these figures it can be seen that the velocity profiles are quite similar, even at differing distances and that it is the temperature profiles which show the greatest differences. Table 5.2 illustrates that Fr_{ing} is a more conservative parameter to identify 1D flow. But as the flow rate goes up, so does the deviation from a 1D profile even though the Froude number is still bigger than 3.2. This suggests that deciding on the interface position solely on the Froude number, might lead to erroneous results as the temperature profile at the interface position deviates from a 1D profile. The next section will try and shed light upon this matter.

5.3 Sensitivity to interface position

The 3D domain used in the reference case is 640m, but this was the result of a number of conservative assumptions. By changing the position of the upstream and downstream interface, it is possible to check if these assumptions were overly conservative and whether it is possible to come up with similar results using a smaller 3D domain. The smaller the 3D domain can be taken, the larger the portion can be that is modelled in 1D, and thus the faster the simulation will finish. Moving both the upstream interface and the downstream interface is considered.

5.3.1 Sensitivity to upstream interface position

Up till now the upstream domain length was taken to be a little over 140m. In the first 70m from the interface, there was no interaction between hot smoke and fresh inflowing air. This was done, to allow the cold flow to fully develop, before interacting with the hot smoke moving in the opposite direction. By moving the upstream interface closer to the fire, it can be evaluated how the upstream domain length influences the results. The upstream interface is moved to x=-76m, just before the back-layering length, and x=-44m, within the back-layering length. Temperature and velocity profiles in steady state, both upstream and downstream are shown in figures 5.15 to 5.18. The profiles are taken at x=-30m and x=50m, since it can be expected, that closer to the fire the influence of the different interface positions is biggest. It can however be seen that there are only minute differences between the profiles for

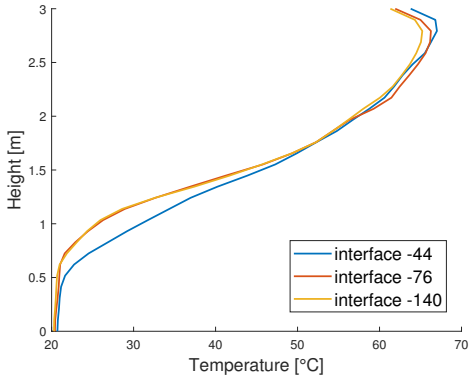

Figure 5.15: Temperature profile -30m

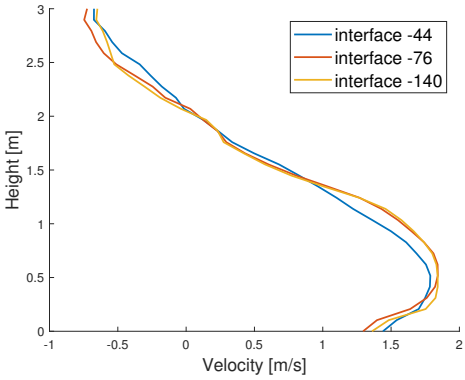

Figure 5.16: Velocity profile -30m

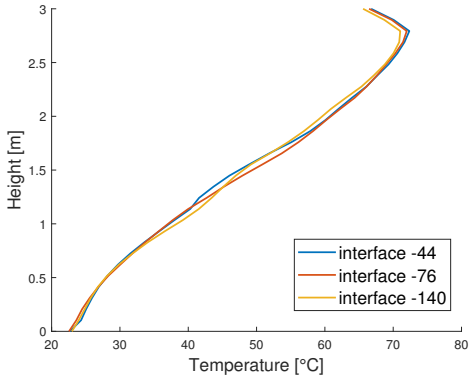

Figure 5.17: Temperature profile 50m

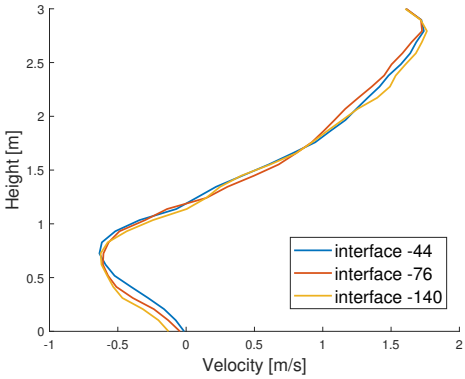

Figure 5.18: Velocity profile 50m

different interface positions. The snapshots in figure 5.19 of smoke spread taken at 300s in Smokeview furthermore show that even before steady state the behaviour of the smoke almost does not differ between simulations with different interface positions.

The simulations prove to be relatively insensitive to the upstream 3D domain length. This relaxes the statement put forward in chapter 4, claiming that the upstream domain length should at least be taken bigger than the back-layering length. The analysis here proves that it is a sufficient but not a necessary condition.

5.3.2 Sensitivity to downstream interface position

The same analysis as performed for the upstream interface position is now performed for the downstream interface position as well. In the previous sections it was seen that as the flow rate goes up, so does the deviation from a 1D profile at the position where Fr_{ing} attains 3.2. Therefore three possible interface positions are suggested here: one where the total deviation from average for the temperature profile is 15%, one where it is 10% and the last suggested position is the one where Fr_{ing} equals 3.2. These positions are given in table 5.3. Since the values for temperature and

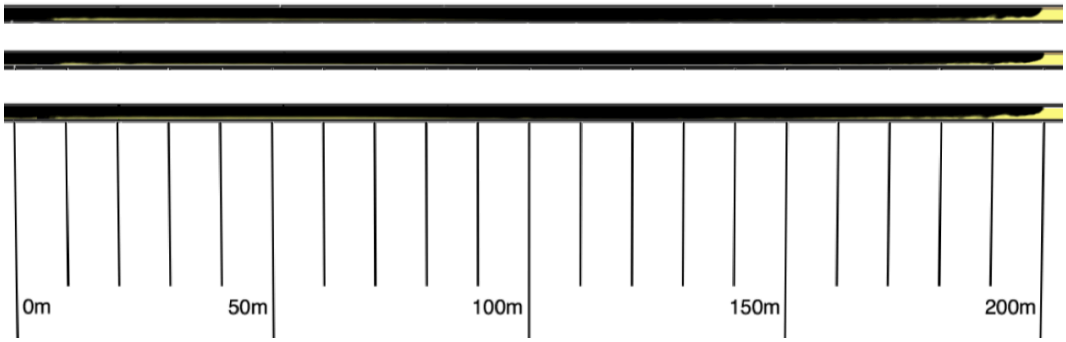

Figure 5.19: Smokeview screenshots showing smoke spread at 300s. Top to bottom: interface at x=-44m, at x=-76m and -140m

	$\Delta T_{max} = 10\%$	$\Delta T_{max} = 15\%$	$Fr_{ing} = 3.2$
$5m^3/s$	$x = 300m \rightarrow 308m$	$x = 250m \rightarrow 244m$	$x = 450m \rightarrow 436m$
$15m^3/s$	$x = 500m \rightarrow 500m$	$x = 400m \rightarrow 404m$	$x = 300m \rightarrow 308m$

Table 5.3: Exact Positions of the downstream interfaces

velocity were only recorded at values of x that were whole multiples of 50 and since the meshes are 32m long, it was not possible to achieve these values exactly, but the next closest values were taken. The analysis is performed, both for the reference case and for the case where the flow rate was increased to $15m^3/s$.

The results shown in figures 5.20 and 5.21 are surprising. They show that there is almost no difference among the calculated temperature profiles if the downstream interface is taken closer to the fire source, even if the deviation from a 1D profile is quite large. In the first case, the total deviation from average is 15% at 250m, while still yielding correct results and in the second case it is even as large as 22% at 300m. This highlights that the inequality $Fr_{ing} > 3.2$ is a sufficient, but not necessary condition to determine the downstream interface position as it is clearly an overly conservative estimate of the needed downstream domain length in the first case.
The question now arises what the limit is for the minimum needed downstream domain length. Plotting the mass flow for the reference case for an interface position of x=244m and x=212 shows that the first signs of instability occur in the simulation with the interface at x=244m, cf. figure 5.22. However the temperature profiles were still correct, as was shown above. When the downstream domain is shortened further up till x=212, the simulation crashes. This suggests that a hard limit is imposed by the numerical stability of the simulation and that every simulation should be looked at on a case by case basis. The domain length suggested by $Fr_{ing} = 3.2$ can be used as an indication, but will lead to overly conservative results in some cases and does not serve as a definite answer on how long the downstream domain should be.

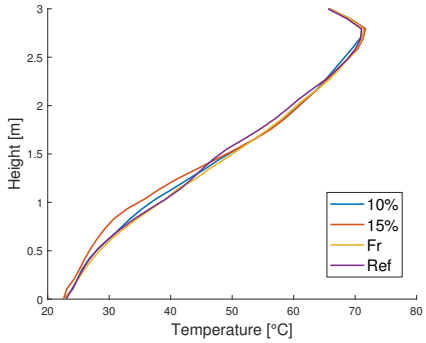

Figure 5.20: Temperature profiles at x=50m for different downstream interface positions and a flow rate of $5^3 m/s$

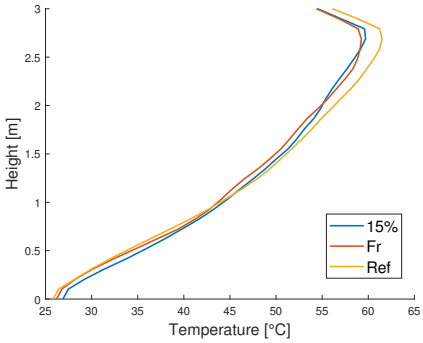

Figure 5.21: Temperature profiles at x=50m for different downstream interface positions and a flow rate of $15^3 m/s$

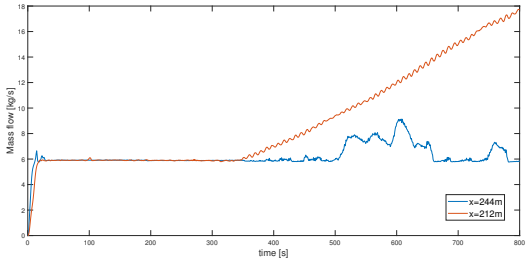

Figure 5.22: Mass flow in the right extraction duct for different downstream interface positions

5.4 Sensitivity to wall boundary conditions

Up till now the walls lining the tunnel were always assumed to be inert. That is, the wall was assumed to stay at a constant ambient temperature. This was based on the assumption that the tunnel and the surrounding ground act as a giant heat sink. In this section, this assumption will be tested. First by comparing the results obtained in the reference case with results obtained by considering the walls to be adiabatic and subsequently by comparing them to results obtained by using 30cm thick concrete walls.

When using an adiabatic boundary condition no heat is exchanged between the moving fluid and the walls and the hot smoke can only cool down by exchanging heat with the colder ambient air. Adiabatic walls are an often used boundary condition in a prescriptive approach as they are supposed to represent a worst-case scenario. In a performance-based approach the emphasis however lies on realistic scenarios and the validity of using adiabatic boundary conditions is refuted. The result of using adiabatic walls is shown by figure 5.23, showing the temperature profile at 450m at

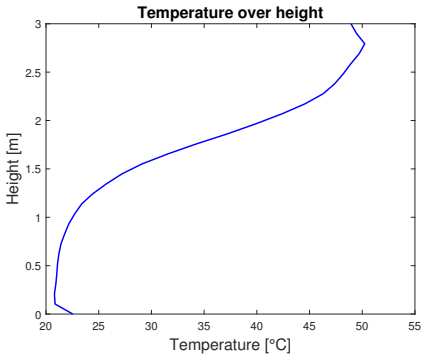

Figure 5.23: Temperature profile at x=450m when using adiabatic walls

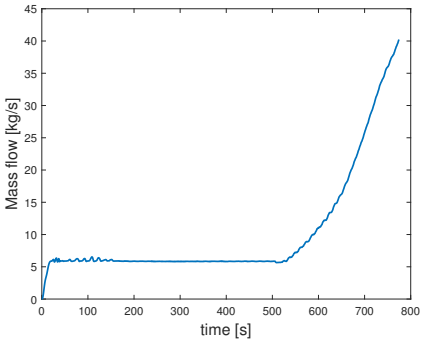

Figure 5.24: Mass flow in the extraction duct when using adiabatic walls

500s. This is right before the smoke reaches the downstream interface at x=500m. From the temperature profile it is evident that there is still strong stratification of the smoke. Indicated as well by $Fr_{ing} = 0.25$ and a total deviation from average of 53 %. Such stratification at a distance of almost 500m from the fire is not to be expected in reality.
The strong stratification also influences the stability of the simulation. As soon as the smoke reaches the 3D-1D interface, the simulation becomes unstable, indicated by a diverging mass flow as shown in 5.24, and eventually it crashes.

As opposed to working with adiabatic walls, using inert walls is the entire other end of the spectrum and could be argued to be not conservative enough. When using inert walls, the hot smoke can transfer as much heat to the walls as it wants, without heating up the wall itself. The wall acts as an infinite heat sink at constant temperature. To evaluate this boundary condition it is compared to walls modelled to represent 30cm thick concrete. The concrete is defined as follows:

```
1  &MATL ID='CONCRETE',
2        CONDUCTIVITY=1.7,
3        SPECIFIC HEAT=0.75,
4        DENSITY=2400./
5
6  &SURF ID='CONCRETE WALL',
7        MATL_ID='CONCRETE',
8        THICKNESS=0.3,
9        ROUGHNESS=0.0005/
```

The resulting temperature profiles are shown both upstream at x=-50m and downstream at x=50m in figures 5.25 and 5.26 respectively. The biggest difference is seen upstream of the fire, where the relative mean deviation between the two profiles is 9%. The higher temperature in the smoke layer also causes the smoke to back-layer a little more than in the case with inert walls. Downstream of the fire the difference between the two profiles is small, with only a mean deviation of 6%.

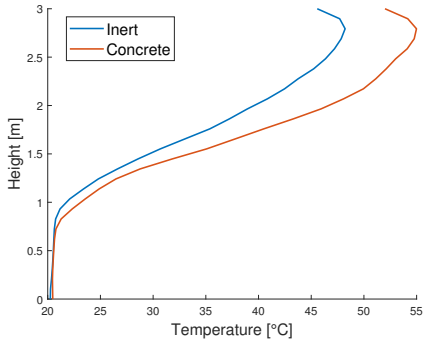

Figure 5.25: Temperature profiles for different wall boundary conditions at x=-50m in steady state

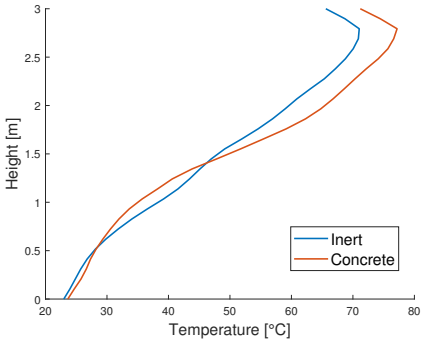

Figure 5.26: Temperature profiles for different wall boundary conditions at x=50m in steady state

Overall the difference between the inert and concrete boundary is small, with the average deviations between the profiles staying under 10%. This shows that when the exact properties of the tunnel lining material are not known the inert boundary condition can serve as a suitable assumption. When more detail is available about the material of course it is better to insert the exact parameters, describing it.

5.5 Summary

This final chapter tested the sensitivity of the reference case that was built up in the previous chapter to several parameters. Both the 1D and 3D domain were considered, with first an extension of the 1D domain to multiple sections. This showed that solely extending the 1D domain did not influence the simulation results when only extraction fans are defined. Following the extension of the 1D domain, the evolution of the Froude number under different flow rates was investigated. The Froude number as defined by Ingason was shown to be more conservative than the one defined by Newman, but as the flow rate increased so did the deviation from a 1D profile. The logical question that followed was what maximum deviation from a 1D profile could serve as indicator for placement of the downstream interface. Unfortunately the results were inconclusive and the only hard limit seemed to be the numerical stability in FDS. The last point that was addressed was the inert boundary condition used throughout this thesis. The analysis in the final section showed that when detailed information on the material properties is not available it serves as a more appropriate condition than adiabatic walls which are often used in prescriptive approaches.

Chapter 6

Conclusion and future work

The LHC accelerator at CERN consists of a complex network of accelerators, tunnels and technical caverns making it almost impossible to model all of the details inside the tunnel exactly. By simplifying the system it was however possible to come up with a multi-scale model of one 3km long section of the LHC tunnel. Rather than exactly representing the tunnel by its horseshoe-shaped cross section, the tunnel was modelled using a rectangular cross section to avoid unrealistic flow patterns, which would be induced by a stair-stepped round tunnel. Following this the ventilation system was also simplified, since the push-pull system employed in the LHC tunnel led to a hyperstatic FDS model. Due to the hyperstatic nature of the exact representation a choice had to be made between an insertion fan only or an extraction fan only system. Eventually an extraction fan was chosen, as to guarantee the exact boundary condition at the downstream 3D-1D interface.
Next on the list was the determination of the needed 3D domain length. By analysing the temperature and velocity profiles resulting from a 1MW polyurethane fire, a 3D domain size of 640m was chosen to form the basis of the reference system. A mesh size of $\delta x \times \delta y \times \delta z = 0.2m \times 0.1m \times 0.1m$ guaranteed as accurate results as practically possible. The choice of the mesh size completed the reference model which acted as a benchmark throughout this thesis.
The first test of the reference case came in the form of an extension of the 1D domain. This showed that solely extending the 1D domain without including extra 3D sections did not influence the results. Next up was a sensitivity study of the flow development with increasing flow rate. Monitoring both the local Froude number as defined by Ingason and as by Newman, indicated that the one defined by Ingason is a more conservative parameter. It was also seen that as the flow rate increased the Froude numbers indicated fully developed flow at positions closer and closer to the fire, but that the deviation from a 1D profile of the temperature profiles also increased.
The logical next step was to use the positions obtained from the Froude numbers to test the sensitivity of the system to different interface positions. It was shown that varying the upstream interface position to well within the back-layering length did not noticeably alter the results. Bringing the downstream interface closer and closer to the fire source did not result in any changes either.

Further analysis of the temperature and velocity profiles could not establish any conclusive evidence that $Fr_{ing} = 3.2$ can serve as an accurate indicator of the necessary downstream interface position, but it was shown that it can serve as a sufficient condition. The only hard limit on the downstream interface was eventually found to be the numerical stability of the simulation.
The last sensitivity study finally showed that if no accurate information is available on the wall lining material, the default inert boundary condition is more appropriate than assuming a worst-case adiabatic wall.

This thesis has tried to present a benchmark system that can be used as long as experimental validation of the results is not available. But it has also shown that a lot more research is needed to make multi-scale modelling a robust alternative to complete 3D modelling. In light of any further research the following improvements are therefore suggested:

A) Investigate the addition of more detail to the tunnel geometry, including vertical ducts that differ in height and adding a more detailed fire source.

B) Include mass storage and heat loss in the 1D ducts.

C) Investigate how a transversal ventilation system could be implemented using the HVAC components.

D) Investigate the effects of adding multiple 3D domains.

E) Further investigate the possibility of using the Fr_{ing} as an indicator for the downstream interface position and the effect of coarsening the mesh upstream and downstream of the fire.

F) Validation of the obtained results via experimental proof or via complete 3D modelling.

A) The tunnel which has been modelled, is a very basic representation of the real LHC tunnel. In reality there are a lot of obstacles and structures inside the tunnel which could influence the development of the flow and alter the velocity and temperature profiles. This is also true for the vertical ventilation ducts. Here these have been assumed to be equal in length, but in reality the topography of the terrain along the surface above the tunnel causes them to be different. This will influence the hydrostatic pressures imposed by them and is expected to influence the mass flow in the simulation. The pressure solver is the workhorse of FDS, but it is also vulnerable to numerical instabilities and changing the elevation of the ducts can have a big influence on this.
The fire used throughout this thesis was a simple 1MW t^2 fire. Questions could and have been raised about the realism of such a fire. A more realistic scenario would be to model for example a cable tray fire, which would cause fire spread along the tunnel. It would be interesting to see how this affects the multi-scale model.

B)The absence of heat transfer in the 1D portion of the multi-scale model was highlighted as one of the main drawbacks in using FDS for multi-scale modelling. A possible workaround was suggested and the practicality of this solution should be further investigated.
Mass storage on the other hand is already included in the FDS source code, but led to stability problems and was not turned on throughout the simulations performed. Further investigation of the cause to this and ways to improve stability are another suggested research topic.

C)The current ventilation system used in the LHC tunnel is a longitudinal system. The goal of a simulation however is to give an accurate idea about possible scenarios. Since it can be assumed that different ventilation systems, such as transversal ventilation, might be employed in future accelerators it is worthwhile investigating how this could be implemented using the HVAC components of FDS.

D) The inclusion of extra sections of 1D domain was shown to not improve the quality of the simulations. The inclusion of extra sections of 3D domains within these section was however not tested. It would be interesting to explore the influence of extra 3D domains on the simulation results. These added 3D domains could for example be used to model the technical caverns along the tunnel or the main caverns which house the detectors along the accelerator ring.

E)Perhaps the main question within a multi-scale model is how long and accurate the 3D domain should be to warrant correct results. That is for there to be no significant difference between the results obtained between a simulation completely modelling the system in 3D and a multi-scale model. An attempt was made to answer this question based on an analysis of both the Froude number and the temperature and velocity profiles over the height of the tunnel. The results were however inconclusive and only identified the Froude number as a sufficient condition. Following the Froude number can as such lead to over-conservative 3D domain lengths and thus increased simulation times. Further research is needed to identify a parameter which can serve as a reliable indicator of the needed 3D domain length. Another possibility which can be looked into to improve simulation times is a coarsening of the 3D mesh further from the fire.

F) The results obtained througout this thesis have been the result of a series of conservative assumptions, but as long as no experimental validation is possible they should be used with caution. A possible intermediate step would be to validate the multi-scale model using a full 3D simulation, considering the computational power available at CERN, this might be a feasible option.

Overall the simulations using the multi-scale model showed results for temperature and velocity profiles which can be expected in reality. A major source of concern was however the stability of the simulations, with seemingly random crashes occurring. These raise the question of how mature multi-scale modelling and perhaps even 3D modelling within FDS is. It should however be remembered that the HVAC modelling functionality was not designed for the purpose of multi-scale modelling of tunnels and it seems that at this moment the usage should be restricted to academic research, as long as experimental validation of the results is not possible.

Bibliography

[1] Ang, C. D. E., Rein, G., Peiro, J., and Harrison, R. (2016). Simulating longitudinal ventilation flows in long tunnels: Comparison of full cfd and multi-scale modelling approaches in FDS6. *Tunnelling and Underground Space Technology*, 52:119 – 126.

[2] Beard, A. and Carvel, R. (2012). *Handbook of Tunnel Fire Safety*. ICE Publishing, second edition.

[3] Brüning, O. S., Collier, P., Lebrun, P., Myers, S., Ostojic, R., Poole, J., and Proudlock, P. (2004a). *LHC Design Report Volume: 1*. CERN Yellow Reports: Monographs. CERN, Geneva.

[4] Brüning, O. S., Collier, P., Lebrun, P., Myers, S., Ostojic, R., Poole, J., and Proudlock, P. (2004b). *LHC Design Report: Volume 2*. CERN Yellow Reports: Monographs. CERN, Geneva.

[5] CERN (2014). The large hadron collider. `https://cds.cern.ch/record/1998498`. [Online; accessed April, 2018].

[6] CERN (2017). CERN Brochure: LHC the guide and FAQ. Education, Communications and Outreach Group.

[7] Colella, F. (2010). *Multiscale modelling of tunnel ventilation flows and fires*. Doctoral dissertation, Politecnico di Turino.

[8] Colella, F., Rein, G., Borchiellini, R., Carvel, R., Torero, J., and Verda, V. (2009). Calculation and design of tunnel ventilation systems using a two-scale modelling approach. *Building and Environment*, 44(12):2357 – 2367.

[9] Colella, F., Rein, G., Borchiellini, R., and Torero, J. L. (2011a). A novel multiscale methodology for simulating tunnel ventilation flows during fires. *Fire Technology*, 47(1):221–253.

[10] Colella, F., Rein, G., Carvel, R., Reszka, P., and Torero, J. (2010). Analysis of the ventilation systems in the dartford tunnels using a multi-scale modelling approach. *Tunnelling and Underground Space Technology*, 25(4):423 – 432.

[11] Colella, F., Rein, G., Verda, V., and Borchiellini, R. (2011b). Multiscale modeling of transient flows from fire and ventilation in long tunnels. *Computers and Fluids*, 51(1):16 – 29.

[12] Cosentino, S. (2017). *Innovative Modeling Approaches for the Design, Operation and Control of Complex Energy Systems with Appliation to Underground infrastructures*. Doctoral dissertation, Politecnico di Turino.

[13] Deardorff, J. W. (1980). Stratocumulus-capped mixed layers derived from a three-dimensional model. *Boundary-Layer Meteorology*, 18(4):495–527.

[14] Floyd, J. (2016). Choosing DT HVAC and MAXIMUM PRESSURE ITERATIONS. Answer given by J. Floyd in FDS discussion group `https://groups.google.com/forum/#!topic/fds-smv/yl1chfQR4gQ`. [Online; accessed April, 2018].

[15] Ingason, H., Li, Y., and Lönnermark, A. (2015). *Tunnel Fire Dynamics*. Springer.

[16] Inigo-Golfin, J. (2009). The LHC HVAC system. Powerpoint presentation. JIG,LHC Performance workshop, Chamonix.

[17] La Mendola, S. (2013). A simplified model for tunnel fire dynamics predictions: validation of a case study. Powerpoint presentation, International Technical Safety Forum, EFSR, Grenoble,France, May 2013.

[18] Li, Y. Z., Lei, B., and Ingason, H. (2010). Study of critical velocity and backlayering length in longitudinally ventilated tunnel fires. *Fire Safety Journal*, 45(6):361 – 370.

[19] McDonough, J. M. (2007). *Introductory lectures on turbulence: Physics, Mathematics and Modeling*. Departments of Mechanical Engineering and Mathematics, University of Kentucky.

[20] McGrattan, K., Hostikka, S., McDermott, R., Floyd, J., Vanella, M., Weinschenk, C., and Overholt, K. (2017a). *Fire Dynamics Simulator Technical Reference Guide volume 1: mathematical model*. NIST.

[21] McGrattan, K., Hostikka, S., McDermott, R., Floyd, J., Vanella, M., Weinschenk, C., and Overholt, K. (2017b). *Fire Dynamics Simulator: user's guide*. NIST.

[22] Newman, J. S. (1984). Experimental evaluation of fire-induced stratification. *Combustion and Flame*, 57(1):33 – 39.

[23] Pope, Stephen, B. (2004). Ten questions concerning the large-eddy simulation of turbulent flows. 6.

[24] Pritchard, P. and Mitchell, J. (2015). *Fox and McDonald's Introduction to Fluid Mechanics, 9th Edition*. Wiley.

[25] Rehm, R. and Baum, H. (1978). The equations of motion for thermally driven, buoyant flows. *Journal of Research of the NBS*, 83:297 – 308.

[26] Rios, O., Arnalich, A., and Mendola, S. L. (2017). FCC brainstorming sessions 1, fire hazard analysis: Berlin baseline evaluation. Powerpoint presentation. HSE, Fire Safety Engineering Team.

[27] Roads and maritime services (2014). *TP04: Road Tunnel Ventilation Systems*. Technical report, Advisory committee on tunnel air quality, NSW government.

[28] Saenen, T., Gielen, R., and Van den Berg, K. (academic year 2013 - 2014). Exercise booklet heat transfer. Addition to the course manual of Heat Transfer, taught by Prof. dr. ir. E. Van den Bulck at the KU Leuven, H08W5A.

[29] Vermesi, I., Rein, G., Colella, F., Valkvist, M., and Jomaas, G. (2017). Reducing the computational requirements for simulating tunnel fires by combining multiscale modelling and multiple processor calculation. *Tunnelling and Underground Space Technology*, 64:146 – 153.

[30] Vermesi, I. M. (2013). *The Feasibility of Multiscale Modelling of Tunnel Fires Using FDS Izabella Melinda Vermesi*. Master thesis, Technical University of Denmark.

Appendices

Appendix A

FDS and Matlab Codes

Basic FDS Code

```
&HEAD CHID='Slice'/
&TIME T_END=800.0/
&MISC DT_HVAC=0.7/
&PRES MAX_PRESSURE_ITERATIONS=1000/


&MESH ID='MESH1',  IJK=160,28,30, XB=-140.0,-108.0,-1.4,1.4,0.0,3.0/
&MESH ID='MESH2',  IJK=160,28,30, XB=-108.0,-76.0,-1.4,1.4,0.0,3.0/
&MESH ID='MESH3',  IJK=160,28,30, XB=-76.0,-44.0,-1.4,1.4,0.0,3.0/
&MESH ID='MESH4',  IJK=160,28,30, XB=-44.0,-12.0,-1.4,1.4,0.0,3.0/
&MESH ID='MESH5',  IJK=160,28,30, XB=-12.0,20.0,-1.4,1.4,0.0,3.0/
&MESH ID='MESH6',  IJK=160,28,30, XB=20.0,52.0,-1.4,1.4,0.0,3.0/
&MESH ID='MESH7',  IJK=160,28,30, XB=52.0,84.0,-1.4,1.4,0.0,3.0/
&MESH ID='MESH8',  IJK=160,28,30, XB=84.0,116.0,-1.4,1.4,0.0,3.0/
&MESH ID='MESH9',  IJK=160,28,30, XB=116.0,148.0,-1.4,1.4,0.0,3.0/
&MESH ID='MESH10', IJK=160,28,30, XB=148.0,180.0,-1.4,1.4,0.0,3.0/
&MESH ID='MESH11', IJK=160,28,30, XB=180.0,212.0,-1.4,1.4,0.0,3.0/
&MESH ID='MESH12', IJK=160,28,30, XB=212.0,244.0,-1.4,1.4,0.0,3.0/
&MESH ID='MESH13', IJK=160,28,30, XB=244.0,276.0,-1.4,1.4,0.0,3.0/
&MESH ID='MESH14', IJK=160,28,30, XB=276.0,308.0,-1.4,1.4,0.0,3.0/
&MESH ID='MESH15', IJK=160,28,30, XB=308.0,340.0,-1.4,1.4,0.0,3.0/
&MESH ID='MESH16', IJK=160,28,30, XB=340.0,372.0,-1.4,1.4,0.0,3.0/
&MESH ID='MESH17', IJK=160,28,30, XB=372.0,404.0,-1.4,1.4,0.0,3.0/
&MESH ID='MESH18', IJK=160,28,30, XB=404.0,436.0,-1.4,1.4,0.0,3.0/
&MESH ID='MESH19', IJK=160,28,30, XB=436.0,468.0,-1.4,1.4,0.0,3.0/
&MESH ID='MESH20', IJK=160,28,30, XB=468.0,500.0,-1.4,1.4,0.0,3.0/

&REAC ID='POLYURETHANE',
FYI='NFPA Babrauskas',
FUEL='REAC_FUEL',
C=6.3,
H=7.1,
O=2.1,
N=1.0,
```

```
35 SOOT_YIELD=0.1,
36 HEAT_OF_COMBUSTION=27000.0/
37
38 &SURF ID='ADIABATICLAYER',
39 COLOR='INVISIBLE',
40 ADIABATIC=.TRUE./
41
42 &SURF ID='FIRE',
43 COLOR='RED',
44 HRRPUA=1000.0,
45 TAU_Q=-50.0/
46
47 &HVAC TYPE_ID='FAN', ID='FanExtr', MAX_FLOW=5., MAX_PRESSURE=2000.,
       ↪ TAU_FAN=50.0/
48
49 &OBST ID='Obstruction', XB=-140.0,-139.9,-1.4,1.4,0.0,3.0, COLOR='GRAY
       ↪  94', OUTLINE=.TRUE., SURF_ID='ADIABATICLAYER'/
50 &OBST ID='Obstruction', XB=499.9,500.0,-1.4,1.4,0.0,3.0, COLOR='GRAY
       ↪ 94', OUTLINE=.TRUE., SURF_ID='ADIABATICLAYER'/
51 &OBST ID='Obstruction', XB=3.5,4.5,-0.5,0.5,0.0,0.1, COLOR='GRAY 94',
       ↪ OUTLINE=.TRUE., SURF_ID='ADIABATICLAYER',DEVC_ID='timer'/
52
53 &VENT ID='left_interface', SURF_ID='HVAC', XB=-139.9,-139.9,-1.4,1.4,0
       ↪ .0,3.0/
54 &VENT ID='right_interface', SURF_ID='HVAC', XB=499.9,499.9,-1.4,1.4,0
       ↪ .0,3.0/
55 &VENT ID='FireVent', SURF_ID='FIRE', XB=3.5,4.5,-0.5,0.5,0.1,0.1, IOR
       ↪ =3, DEVC_ID='timer'/
56
57 z-nodes:
58 &HVAC ID='NodeInsertion100', TYPE_ID='NODE', DUCT_ID='DuctInsertion',
       ↪ AMBIENT=.TRUE., XYZ=-1500.0,0.0,100.0/
59 &HVAC ID='NodeRightExtraction100', TYPE_ID='NODE', DUCT_ID='
       ↪ DuctRightExtractionFan', AMBIENT=.TRUE., XYZ=1500.0,0.0,100.0/
60 &HVAC ID='NodeRightExtraction99', TYPE_ID='NODE', DUCT_ID='
       ↪ DuctRightExtractionFan','DuctRightExtraction', XYZ=1500.0,0.0
       ↪ ,99.0/
61
62 % interface nodes:
63 &HVAC ID='NodeRightInterface', TYPE_ID='NODE', DUCT_ID='
       ↪ Duct_RightInterf_1500m', VENT_ID='right_interface'/
64 &HVAC ID='NodeLeftInterface', TYPE_ID='NODE', DUCT_ID='
       ↪ Duct_LeftInterf_-1500m', VENT_ID='left_interface'/
65
66 % x-nodes:
67 &HVAC ID='Node_1500m', TYPE_ID='NODE', DUCT_ID='Duct_RightInterf_1500m
       ↪ ','DuctRightExtraction',XYZ=1500.0,0.0,1.5/
68 &HVAC ID='Node_-1500m', TYPE_ID='NODE', DUCT_ID='DuctInsertion','
       ↪ Duct_LeftInterf_-1500m', XYZ=-1500.0,0.0,1.5/
69
70
71 % vertical ducts:
72 &HVAC ID='DuctInsertion', TYPE_ID='DUCT', DIAMETER=2.9, NODE_ID='
       ↪ NodeInsertion100','Node_-1500m', ROUGHNESS=5.0E-5, LENGTH=98.5/
```

```
&HVAC ID='DuctRightExtraction', TYPE_ID='DUCT', DIAMETER=2.9, NODE_ID=
    ↪ 'Node_1500m','NodeRightExtraction99', ROUGHNESS=5.0E-5, LENGTH
    ↪ =97.5/
&HVAC ID='DuctRightExtractionFan', TYPE_ID='DUCT', DIAMETER=2.9,
    ↪ FAN_ID='FanExtr', NODE_ID='NodeRightExtraction99','
    ↪ NodeRightExtraction100', ROUGHNESS=5.0E-5, LENGTH=1/


% horizontal ducts:
&HVAC ID='Duct_RightInterf_1500m', TYPE_ID='DUCT', AREA=8.4, PERIMETER
    ↪ =2.9, NODE_ID='NodeRightInterface','Node_1500m', ROUGHNESS=5.0E
    ↪ -4, LENGTH=1360.1/
&HVAC ID='Duct_LeftInterf_-1500m', TYPE_ID='DUCT', AREA=8.4, PERIMETER
    ↪ =2.9, NODE_ID='Node_-1500m','NodeLeftInterface', ROUGHNESS=5.0E
    ↪ -4, LENGTH=1000.1/


% Devices:
&DEVC ID='timer', XYZ=0.0,0.0,0.0, QUANTITY='TIME', SETPOINT=100.0,
    ↪ INITIAL_STATE=.FALSE./

&DEVC ID='DuctTemp_RightInterf_1500', QUANTITY='DUCT TEMPERATURE',
    ↪ DUCT_ID='Duct_RightInterf_1500m'/
&DEVC ID='DuctTemp_LeftInterf_-1500', QUANTITY='DUCT TEMPERATURE',
    ↪ DUCT_ID='Duct_LeftInterf_-1500m'/
&DEVC ID='DuctTemp_RightExtraction', QUANTITY='DUCT TEMPERATURE',
    ↪ DUCT_ID='DuctRightExtraction'/

&DEVC ID='SootFrac_1500', QUANTITY='NODE MASS FRACTION', NODE_ID='
    ↪ Node_1500m', SPEC_ID='SOOT'/

&DEVC ID='MFlow_RightExtraction', QUANTITY='DUCT MASS FLOW', DUCT_ID='
    ↪ DuctRightExtraction'/
&DEVC ID='Mflow_Insertion', QUANTITY='DUCT MASS FLOW', DUCT_ID='
    ↪ DuctInsertion'/

&DEVC ID='VFlow_RightExtraction', QUANTITY='DUCT VOLUME FLOW', DUCT_ID
    ↪ ='DuctRightExtraction'/
&DEVC ID='Vflow_Insertion', QUANTITY='DUCT VOLUME FLOW', DUCT_ID='
    ↪ DuctInsertion'/

&DEVC ID='P_RightInterface', QUANTITY='NODE PRESSURE', NODE_ID='
    ↪ NodeRightInterface'/
&DEVC ID='P_LeftInterface', QUANTITY='NODE PRESSURE', NODE_ID='
    ↪ NodeLeftInterface'/
&DEVC ID='P_1500m', QUANTITY='NODE PRESSURE', NODE_ID='Node_1500m'/
&DEVC ID='P_-1500m', QUANTITY='NODE PRESSURE', NODE_ID='Node_-1500m'/
&DEVC ID='P_Insert100', QUANTITY='NODE PRESSURE', NODE_ID='
    ↪ NodeInsertion100'/
&DEVC ID='P_RightExtr99', QUANTITY='NODE PRESSURE', NODE_ID='
    ↪ NodeRightExtraction99'/

% Temperature profiles
&DEVC XB=4.0,4.0,0.0,0.0,0.0,3.0, QUANTITY='TEMPERATURE', ID='Temp_10'
    ↪ , POINTS=30,TIME_HISTORY=.TRUE./
```

```
106 &DEVC XB=20.0,20.0,0.0,0.0,0.0,3.0, QUANTITY='TEMPERATURE', ID='
    ↪ Temp_20', POINTS=30,TIME_HISTORY=.TRUE./
107
108                         etc ...
109
110 &DEVC XB=-10.0,-10.0,0.0,0.0,0.0,3.0, QUANTITY='TEMPERATURE', ID='
    ↪ Temp_-10', POINTS=30,TIME_HISTORY=.TRUE./
111 &DEVC XB=-30.0,-30.0,0.0,0.0,0.0,3.0, QUANTITY='TEMPERATURE', ID='
    ↪ Temp_-30', POINTS=30,TIME_HISTORY=.TRUE./
112
113                         etc...
114
115
116 % Velocity profiles
117 &DEVC XB=20.0,20.0,0.0,0.0,0.0,3.0, QUANTITY='U-VELOCITY', ID='Vel_20'
    ↪ , POINTS=30,TIME_HISTORY=.TRUE./
118 &DEVC XB=50.0,50.0,0.0,0.0,0.0,3.0, QUANTITY='U-VELOCITY', ID='Vel_50'
    ↪ , POINTS=30,TIME_HISTORY=.TRUE./
119
120                         etc...
121
122
123 &DEVC XB=-10.0,-10.0,0.0,0.0,0.0,3.0, QUANTITY='U-VELOCITY', ID='Vel_
    ↪ -10', POINTS=30,TIME_HISTORY=.TRUE./
124 &DEVC XB=-30.0,-30.0,0.0,0.0,0.0,3.0, QUANTITY='U-VELOCITY', ID='Vel_
    ↪ -30', POINTS=30,TIME_HISTORY=.TRUE./
125
126                         etc...
127
128 % Pressure profile
129 &DEVC XB=-139.0,499.0,0.0,0.0,1.5,1.5, QUANTITY='PRESSURE', ID='
    ↪ Press_1.5', POINTS=65,TIME_HISTORY=.TRUE./
130
131 % Soot profile
132 &DEVC XB=-139.0,499.0,0.0,0.0,1.5,1.5, QUANTITY='VOLUME FRACTION',
    ↪ SPEC_ID='SOOT',ID='Soot_1.5', POINTS=33,TIME_HISTORY=.TRUE./
133
134 &TAIL /
135
136 }
```

Matlab code

Froude number calculation

```
function [froudeNrIng,froudeNrNM] = FroudeNumber(FileName,time,Location,timeSpan)

%FROUDENUMBER Determines the Froude number as defined originally by Newman,
%but also as defined by Ingason in the Tunnel fire safety handbook;
%
%   output: [froude number as defined by Ingason, froude number as defined by Newman]
%   input: (csv output file, time, location, time span over which variables are averaged before being input in the formula)
%
% author: Melchior Schepers                                date: 1/4/2018


H=3;
g=9.81;
[timeAverageVel]=AverageData(FileName,'Velocity',time,Location,timeSpan);
[timeAverageTemp]=AverageData(FileName,'Temperature',time,Location,timeSpan);
averageVel=mean(timeAverageVel,2)
averageTemp=mean(timeAverageTemp,2)+273
deltaTCF=timeAverageTemp(1,27)-timeAverageTemp(1,4)
deltaTavg=averageTemp-293
froudeNrIng=(averageVel.*averageTemp./293).^2./(1.5.*g.*H.*deltaTavg./averageTemp);
froudeNrNM=(averageVel.*averageTemp./293).^2./(g.*H.*deltaTCF./averageTemp);
end
```

```
function [averagedData]=AverageData(FileName,Parameter,time,Location,timeSpan)

% Author: Melchior Schepers                 Date:14/03/2018
% Function to easily plot the results from an FDS analysis which
% uses an array of devices.
%
% The variables in the FDS script need to be of the form:
% BasicName_Location-DeviceNumber
% (-DeviceNumber is appended automatically by specifying an array of devices in FDS)
% inputs: Filename, Parameter to plot, time, location,time span over which to average
% ouput:  Averaged data
%
% Basic parameters to be set inside the funtion
```

```
14
15 %% set basic parameters
16 NumberOfPressDevc=65;
17 NumberOfTempDevc=30;
18 NumberOfVelDevc=30;
19 FireLocation=144; % Only necessary if you want to plot the fire
       ↪ location in the pressure profile graph
20 TunnelLength=640;
21 height = 3;
22 dash = '-';
23
24 %% Crunch the numbers
25 [data,header] = xlsread(FileName);
26 t=data(:,1);
27 [time_value,time_index]=min(abs(t-time));    %select time value
       ↪ closest to the wanted value
28 [time_value2,time_index2]=min(abs(t-(time-timeSpan)));
29
30 if strcmp(Parameter,'Temperature')
31     ShortParam='Temp_';                      %basic name of parameter
           ↪ in fds script
32     Dimensions=strcat('[',char(176),'C',']');
33     NumOfDev=NumberOfTempDevc;
34     flag=1;
35 elseif strcmp(Parameter,'Velocity')
36     ShortParam='Vel_';                       %basic name of parameter
           ↪ in fds script
37     Dimensions='[m/s]';
38     NumOfDev=NumberOfVelDevc;
39     flag=2;
40 elseif strcmp(Parameter,'Pressure')
41     ShortParam='Press_';                     %basic name of parameter
           ↪ in fds script
42     Dimensions='[Pa]';
43     NumOfDev=NumberOfPressDevc;
44     flag=3;
45 else
46     disp('No such parameter')
47     return;
48 end
49
50     CurrentString=strcat(ShortParam,Location,dash);
51     for k=1:NumOfDev
52         if (k<=9)                            %if loop is necessary to
               ↪ append leading zero to first 9 devices
53         l=num2str(k);
54         HeaderToMatch=strcat(CurrentString,'0',l);
55         column = find(strcmp(header(2,:),HeaderToMatch));
56         FDSData(:,k)=data(:,column);
57
58         else
59         l=num2str(k);
60         HeaderToMatch=strcat(CurrentString,l);
61         column = find(strcmp(header(2,:),HeaderToMatch));
62         FDSData(:,k)=data(:,column);
```

```
63          end
64      end
65
66      A=FDSData(time_index2:time_index,:);
67      averagedData=mean(A);
```

Appendix B

Time averaging and percentual metrics

Time averaging

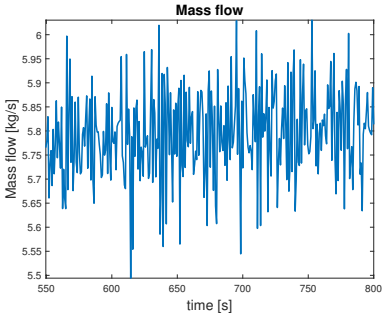

Figure B.1: Mass flow from 550s-800s

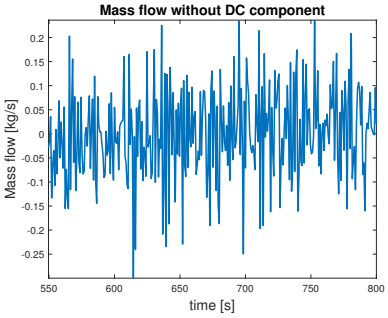

Figure B.2: Mass flow from 550s-800s with average substracted

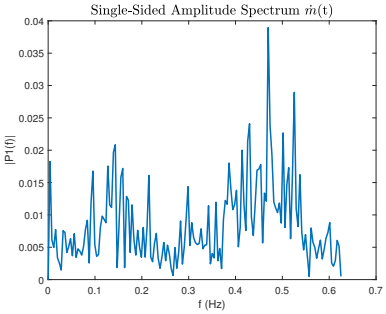

Figure B.3: Amplitude spectrum of the mass flow time series

The mass flow is observed to reach steady state at 550s for the reference case.

Removing the DC-component from the signal in figure B.1 results in figure B.2. By performing a FFT the frequency spectrum of this signal can be analysed as shown in figure B.3. No clear frequency component stands out, except for a small peak at around 0.47Hz, but in general the signal is quite noisy. The highest frequency is situated at 0.625Hz, thus a period of 1.6s. This is not unexpected since the DEVC outputs in fds were written out every 0.8s.
Since the time period of the highest frequency is 1.6, averaging over 15s allows to roughly take into account 10 time periods to smoothen out instabilities.

Percentual metrics

Two percentual metrics are defined and used in this thesis. One indicating the relative total deviation from average, which is used as a metric to identify the deviation from a 1D profile. The other is the relative mean deviation over a velocity or temperature profile. This is used when comparing two temperature profiles against each other. They are defined as follows:

Relative total deviation from average

The relative total deviation from average is defined as follows:

$$\Delta X_{max} = \frac{max(X_1) - min(X_1)}{mean(X_1)}$$

With X_1 the vector containing the discrete values of the profile.

This definition allows to incorporate both the relative difference from average for the minimum value as for the maximum value. This is based on the assumption that for the profile to become 1D, the cold and hot portion have to mix and thus both have to move towards the average value.

Relative mean deviation

The relative mean deviation is defined as the mean of the percentual deviation of the considered profile with respect to the reference profile:

$$\Delta X_{avg} = \frac{1}{n} \sum_{i=1}^{n} \frac{|X_{2,i} - X_{1,i}|}{X_{1,i}}$$

With X_1 and X_2 the n-dimensional vectors containing the discrete values of the profiles. If X_2 is not n-dimensional, linear interpolation is used to make it n-dimensional.

Appendix C

Computational characteristics

Chapter 4: reference case

simulation	# cells per mesh	# meshes	total # cells	cores per mesh	core -hours	DT HVAC	Nodes
Insertion fan only	$160 \times 28 \times 30$	20	2 688 000	8	2556.9	0.7	batch-long
Extraction fan only	$160 \times 28 \times 30$	20	2 688 000	8	2987.1	0.7	be-short
coarse	$64 \times 7 \times 6$	20	53 760	8	14.24	0	be-short
medium	$160 \times 14 \times 15$	20	672 000	8	338	0	be-short
fine	$160 \times 28 \times 30$	20	2 688 000	8	2987.1	0.7	be-short

Chapter 5: sensitivity studies

simulation	# cells per mesh	# meshes	total # cells	cores per mesh	core -hours	DT HVAC	Nodes
Extended system insertion	$160 \times 28 \times 30$	20	2 688 000	8	NA	0.7	batch-long
Extended system extraction	$160 \times 28 \times 30$	20	2 688 000	8	2998.7	0.7	be-short
$\mathbf{10 m^3/s}$	$160 \times 28 \times 30$	20	2 688 000	8	2500.4	0.7	batch-long
$\mathbf{15 m^3/s}$	$160 \times 28 \times 30$	20	2 688 000	8	2689.3	0.7	batch-long
$\mathbf{20 m^3/s}$	$160 \times 28 \times 30$	20	2 688 000	8	3018.7	0.7	be-short

simulation	# cells per mesh	# meshes	total # cells	cores per mesh	core -hours	DT HVAC	Nodes
$x = -44m$	$160 \times 28 \times 30$	17	2 254 800	8	2729.3	0.7	be-short
$x = -76m$	$160 \times 28 \times 30$	18	2 419 200	8	2901.3	0.7	be-short
$5m^3/s$ $x = 244m$	$160 \times 28 \times 30$	12	1 612 800	8	2399.1	0.7	be-short
$5m^3/s$ $x = 308m$	$160 \times 28 \times 30$	14	1 881 600	8	2524	0.7	be-short
$5m^3/s$ $x = 436m$	$160 \times 28 \times 30$	18	2 419 200	8	2771.1	0	be-short
$15m^3/s$ $x = 308m$	$160 \times 28 \times 30$	14	1 881 600	8	2487.6	0.7	batch-long
$15m^3/s$ $x = 404m$	$160 \times 28 \times 30$	17	2 284 800	8	2626.6	0	batch-long
concrete	$160 \times 28 \times 30$	20	2 688 000	8	2799.6	0	be-short
adiabatic	$160 \times 28 \times 30$	20	2 688 000	8	NA	0.7	be-short

Appendix D

Best practices when using HVAC modelling in FDS

The info gathered in this appendix, stems from personal experience gathered over the course of this thesis. But most, if not all, of the information can also be found throughout the FDS user guide, albeit perhaps not grouped together as here.

The low mach number approximation used in FDS causes pressure variations to occur immediately throughout the entire 3D domain, which is unrealistic in long tunnels and easily leads to numerical instabilities. To allow the solver to try and match the old and new pressure fields during every time step the value of MAX_PRESSURE_ITERATIONS can be augmented from the default value of 10 in order to allow the solver more time to converge. In this thesis a value of 1000 was used. Use with caution as this can lead to excessive simulation times.

If the simulation crashes for unclear reasons, the following can be tried to resurrect the situation

- Change the grid size.
- Change the flow rate by at least $0.4m^3/s$.
- Omit or try varying the DT_HVAC parameter.
- Avoid sudden changes in duct cross section, try using one single cross section throughout the entire domain.
- Pay attention to changes in height as both background pressure and ambient temperature change over height. Try getting the simulation to work with all nodes at the same height first.
- Do not forget to specify a roughness or loss coefficient inside the ducts.
- Specify a quadratic fan rather than a constant volumetric fan.

- Try using a different pressure solver, e.g. GLMAT
- Check if the simulation runs without a fire.
- Monitoring mass flow and pressure inside the 3D domain can usually give a good indication at which point the instability occurs.